

Cite this: *J. Mater. Chem. A*, 2020, **8**, 21503

## Indoor application of emerging photovoltaics—progress, challenges and perspectives

Xueyan Hou,<sup>†a</sup> Yiwen Wang,<sup>ID †a</sup> Harrison Ka Hin Lee,<sup>ID \*b</sup> Ram Datt,<sup>b</sup> Nicolas Uslar Miano,<sup>a</sup> Dong Yan,<sup>a</sup> Meng Li,<sup>ID c</sup> Furong Zhu,<sup>ID d</sup> Bo Hou,<sup>ID e</sup> Wing Chung Tsoi<sup>ID \*b</sup> and Zhe Li<sup>ID \*a</sup>

The development of solution-processed photovoltaic (PV) devices for indoor applications has recently attracted widespread attention owing to their outstanding potential in harvesting energy efficiently for low-power-consumption electronic devices, such as wireless sensors and internet of things (IoT). In particular, organic PVs (OPVs), perovskite PVs (PPVs) and quantum dot PVs (QDPVs) are among the most promising emerging photovoltaic technologies that have already demonstrated strong commercialisation potential for this new market, owing to their excellent yet highly tuneable optoelectronic properties to meet the demands for specific applications. In this review, we summarise the recent progress in the development of OPVs, PPVs and QDPVs for indoor applications, showing the rapid advances in their device performance in conjunction with highly diverse materials and device designs, including semi-transparent, flexible and large-area devices. The remaining challenges of these emerging indoor PV technologies that need to be urgently addressed toward their commercialisation, including, in particular, their limited stability and high ecotoxicity, will be discussed in detail. Potential strategies to address these challenges will also be proposed.

Received 16th July 2020  
Accepted 21st September 2020

DOI: 10.1039/d0ta06950g

rsc.li/materials-a

<sup>a</sup>School of Engineering and Materials Science, Queen Mary University of London, London, E1 4NS, UK. E-mail: zhe.li@qmul.ac.uk<sup>b</sup>SPECIFIC, College of Engineering, Bay Campus, Swansea University, Swansea, SA1 8EN, UK. E-mail: k.h.lee@swansea.ac.uk; w.c.tsoi@swansea.ac.uk<sup>c</sup>Helmholtz-Zentrum Berlin für Materialien und Energie, Kekuléstraße 5, 12489 Berlin, Germany<sup>d</sup>Department of Physics, Research Centre of Excellence for Organic Electronics and Institute of Advanced Materials, Hong Kong Baptist University, Kowloon Tong, Hong Kong, China<sup>e</sup>Condensed Matter and Photonics Group, School of Physics and Astronomy, Cardiff University, Cardiff, CF24 3AA, UK

† These authors contribute equally.



Dr Xueyan Hou received her PhD degree (2019) from the School of Physics and Astronomy at Queen Mary University of London under the supervision of Dr John Dennis and Prof. Jenny Nelson from Imperial College London. Her PhD work was about the organic solar cells based on single isomers of high-adducts fullerene. She then worked as a postdoctoral research associate at the School of Engi-

neering and Materials Sciences, Queen Mary University of London with research interests in the field of stability study of solution-processed solar cells.



Dr Yiwen Wang is currently a Postdoctoral Research Assistant in the School of Engineering and Materials Science at Queen Mary University of London. She received her BSc in optoelectronics from Taiyuan University of Technology in 2015. She obtained her MSc and PhD in Physics from Hong Kong Baptist University in 2016 and 2019, respectively. Her research interests include organic photovol-

taic cells for indoor application and the stability of nonfullerene organic solar cells.



# 1 Introduction

In the past few years, indoor photovoltaics (PVs) have attracted intense research attention due to their potential in harvesting indoor light energy efficiently to drive low-power consumption electronic devices such as indoor sensors and internet of things (IoT). This market represents a substantial promise for future growth with huge societal benefits, as it offers a highly innovative and feasible solution for power generating windowpanes, mitigates tedious battery replacement tasks and helps to build smart homes, offices and buildings. Crystalline silicon (c-Si) PV cells, which have dominated the outdoor solar cell markets to date, are an advisable candidate that can be transferred into the indoor PV market quickly. However, the absorbance of crystalline silicon PV cells (bandgap  $\sim 1.1$  eV) does not match the spectrum of the majority of daily used indoor light sources

nowadays such as fluorescent lamps (FLs) and light-emitting diodes (LEDs), the emissions of which are mainly in the region of 380–740 nm.<sup>1,2</sup> Microcrystalline Si (m-Si) and amorphous Si (a-Si), which typically possess a higher bandgap of up to 2.1 eV, usually exhibit only modest power conversion efficiency (PCE) due to increased defects.<sup>3–5</sup> PV devices made with III–V compound semiconductors typically exhibit a higher PCE than crystalline silicon under low light, owing to a better match of their absorbance to the spectrum of indoor light sources and higher open-circuit voltage ( $V_{oc}$ ). For example, a single-junction InGaP cell, with a bandgap of  $\sim 1.9$  eV, can exhibit a PCE of 30% under indoor conditions upon optimisation of doping levels and active layer thickness.<sup>6</sup> However, PV devices based on III–V semiconductors are relatively less popular due to their high sensitivity to structural defects, making it a necessity for them to be manufactured under strictly controlled conditions



*Dr Harrison Ka Hin Lee received his BSc in Physics and PhD under the supervision of Prof. Shu Kong So from Hong Kong Baptist University in 2010 and 2015, respectively. He then moved to Swansea University as a Technology Transfer Fellow. His research interests include organic and perovskite photovoltaics for indoor and aerospace applications, semi-transparent devices, their optoelectronic properties, and their stability.*



*Dr Wing Chung Tsoi is a Senior Lecturer at the Materials Research Centre, College of Engineering, Swansea University. He obtained his PhD from the University of Hull, and did his postdoctoral research at Sheffield University, Imperial College and National Physical Laboratory (UK). His research interests include organic and perovskite photovoltaic cells for indoor and aerospace applica-*

*tions, organic semi-transparent solar cells, their stability and advanced characterization techniques to study optoelectronic devices. Dr Tsoi has published 69 papers, given 25 invited talks and was just awarded the Royal Microscopy Society Medal for Innovation in Applied Microscopy for Engineering and Physical Sciences.*

*tions, organic semi-transparent solar cells, their stability and advanced characterization techniques to study optoelectronic devices. Dr Tsoi has published 69 papers, given 25 invited talks and was just awarded the Royal Microscopy Society Medal for Innovation in Applied Microscopy for Engineering and Physical Sciences.*



*Dr Bo Hou is a Lecturer in the School of Physics and Astronomy, at Cardiff University. He received his PhD degree from the University of Bristol (2010–2014). He worked as a postdoctoral researcher at the University of Oxford (2014–2018, Wolfson College) and a Senior Research Fellow at the University of Cambridge (2018–2020, St Edmund's College). His research interests include QD*

*synthesis, QD solar cells, QD optoelectronics, electron microscopy (TEM) and dynamic charge transfer analysis.*



*Dr Zhe Li is a Senior Lecturer in Materials Science at the School of Engineering and Materials Science, Queen Mary University of London. He received his PhD from Cavendish Laboratory at the University of Cambridge in 2012, and worked as a research associate/research fellow/junior group leader at Imperial College London (2012–2015) and Swansea University (2015–2017) and as a Lecturer of*

*Energy Materials at School of Engineering, Cardiff University (2018–2019). His main research interest includes organic, perovskite and quantum dot photovoltaic cells, including emerging target applications, stability analysis and advanced materials and device characterisation.*



including the use of high temperature and high-vacuum epitaxial deposition processes, leading to a high fabrication cost.

Recently, there has been significant progress in the development of high-performance solution-processed solar cells based on printable PV materials, such as organic, perovskite and quantum dot (QD) semiconductors. This class of PV technology differs from conventional silicon and III–V compound semiconductor PV technologies in that they are typically lightweight, flexible, versatile and inexpensive, with exceptional compatibility, low capex, high throughput manufacturing and a remarkably quick energy payback time as low as 1.8 to 2.4 months (in comparison to ~2.3 years for the typical GaAs III–V compound PV semiconductor, ~1.1 years for a Si PV device and ~2 years for m-Si and c-Si PVs).<sup>7,8</sup> While the rapid advances in their materials and device design have already led to outstanding performances under outdoor conditions (e.g. AM1.5G irradiation), there has been increasing research prevalence in the development of solution-processed organic PV (OPV), perovskite PV (PPV) and quantum dot PV (QDPV) devices for indoor applications. For example, impressive efficiencies of over 31% for OPV cells,<sup>9</sup> over 37% for PPV cells<sup>10</sup> and over 20% for QDPV cells<sup>11</sup> under various low light conditions have recently been achieved, already competing with their conventional inorganic counterparts. In addition, the indoor PV market is increasing rapidly with an estimated market size of \$850 million by 2023, which may further reach \$10 billion in the following years.<sup>12</sup> In the meantime, the manufacturing cost of emerging PV technologies is becoming highly competitive, with the manufacturing cost of OPVs and PPVs estimated at 50 and 31.7 \$ per m<sup>2</sup> respectively,<sup>13,14</sup> compared to a manufacturing cost of ~76 and 160 \$ per m<sup>2</sup> for c-Si and III–V compound PVs.<sup>15</sup> It should be noted, however, that the cost of emerging indoor PVs strongly depends on their manufacturing yield, currently at an estimated cost of ~100 \$ per m<sup>2</sup> limited by the expected indoor PV market size in 2018–2023.<sup>12</sup>

However, several remaining challenges still need to be overcome in order to achieve the commercialisation of OPVs, PPVs and QDPVs for indoor applications, despite their already impressive device performances. The drastically different operating environments of indoor PVs compared to outdoor PVs, in particular, in light and heat stress, may lead to different degradation mechanisms driven by different environmental stress factors, which need to be fully understood and mitigated in order to achieve long-term device stability. The potentially high ecotoxicity of perovskite PVs and QDPVs, primarily due to their reliance on harmful substances (such as lead) to function efficiently, may impose a high risk for indoor applications owing to a higher degree of overlap of indoor PVs with human life. In this review, we summarise the recent scientific progress made in materials and device design resulting in the rapid development of high-performance OPV, PPV and QDPV devices for indoor applications, including a range of device structures such as semi-transparent, flexible and large-area devices. We further summarise a number of major scientific and industrial challenges that remain to be addressed toward the commercialisation of these emerging technologies, including the urgent

need to significantly enhance their operational stability and reduce their ecotoxicity. We highlight our perspectives in the potential strategies to address these challenges, which will also be discussed in detail. By overcoming these challenges, it is reasonable to believe that these indoor PV technologies will realise their full potential for commercialisation in the near future.

## 2 Recent progress

### 2.1 OPV for indoor application

**2.1.1 Performance improvement methods.** OPVs have recently been established as a highly promising candidate for efficient indoor light-harvesting devices. Compared to their silicon-based counterparts, their optical absorbance can be optimised to match the emission of artificial light sources such as LEDs and FL through adjustment of their molecular structures. For example, a range of highly efficient polymer:fullerene and polymer:nonfullerene based blend systems with excellent spectral matches have recently been developed for indoor applications, achieving PCEs of over 17% under 1 sun illumination<sup>16</sup> and over 26% under 1000 illuminance (lx) LED light, with a predicted PCE of over 40% achievable with a minimum energy loss of 0.5 eV at a bandgap of 1.80 eV under low light conditions.<sup>17</sup>

There have been extensive investigations into the key factors determining the indoor performance of OPV devices in recent years. It has been reported that a shunt resistance ( $R_{sh}$ ) of larger than 85 k $\Omega$  cm<sup>2</sup> is required to achieve high-performance P3HT:PCBM devices under low light owing to suppressed dark current ( $J_D$ ) and reduced loss in  $V_{oc}$ , while series resistance ( $R_s$ ) has a relatively minor effect,<sup>18</sup> indicating that a sufficiently large  $R_{sh}$  is an important consideration to ensure the efficient operation of OPVs under low light conditions. Lechêne *et al.* reported that the ratio of  $J_D$  to short-circuit current ( $J_{sc}$ ) under 1 sun is a more comprehensive criterion than  $R_{sh}$  alone in determining the device performance of OPVs under low light. Lechêne *et al.* further proposed an empirical equation to evaluate the potential of indoor OPVs, expressed by  $\frac{J_D}{J_{sc}} \cong \frac{P_{min}}{P_{1\ sun}}$ , (where  $P_{min}$  is the minimal light power and  $P_{1\ sun}$  is the light power under 1 sun condition), assuming a device current that is proportional with light intensity.<sup>19</sup>

It was further found that  $V_{oc}$  plays an important role in the operation of OPVs under low light conditions since  $V_{oc}$  follows a logarithmic relationship with light intensity ( $I$ ) expressed by  $V_{oc} \sim \frac{nkT}{q} \ln I$  (where  $q$  is the elementary charge,  $k$  is the Boltzmann's constant,  $T$  is absolute temperature, and  $n$  is the diode ideality factor),<sup>20–22</sup> which decreases with decreasing light intensity.<sup>23–25</sup> Therefore, ensuring a high  $V_{oc}$  under 1 sun, in conjunction with an ideality factor  $n$  close to 1, is a critical consideration to achieve high  $V_{oc}$  and therefore high device performance under low light conditions.<sup>16</sup> Yang *et al.* investigated the device performance of various OPV blend systems under both white LED and fluorescent illuminations, and also found that the devices with higher  $V_{oc}$  values under 1 sun generally exhibit





Fig. 1 (a) Energy level diagram,  $J$ - $V$  characteristics under 1 sun and LED 1000 lx illumination of the devices with different polymer:PC<sub>71</sub>BM blend systems. Reproduced from ref. 27 with permission from WILEY-VCH. (b) Energy level diagram,  $J$ - $V$  characteristics under 1 sun of the devices with different PBDB-TF:acceptor blend systems and  $J$ - $V$  characteristics of PBDB-TF:ITCC-based devices under LED with different light intensities. Reproduced from ref. 28 with permission from WILEY-VCH. (c) Energy level diagram,  $J$ - $V$  characteristics under 1 sun and FL 1000 lx of the devices with CD1:PBN-10 and CD1:ITIC blend systems. Reproduced from ref. 30 with permission from The Royal Society of Chemistry.

higher performance under low light (up to 13.76% at 500 lx, Fig. 1a).<sup>26</sup> More recently, much effort has been made on enhancing  $V_{oc}$  for indoor OPVs through controlling the donor-acceptor energetics, *i.e.* the effective bandgap which is the energy level difference between the lowest unoccupied molecular orbital (LUMO) of the acceptor and the highest occupied molecular orbital (HOMO) of the donor. Based on a deep-HOMO PDTBTBz-2F<sub>anti</sub> donor and a PC<sub>71</sub>BM acceptor, You *et al.* obtained a high  $V_{oc}$  of 0.817 V and an outstanding PCE of 23.1% under 1000 lx

LED illumination, surpassing the other polymer:PC<sub>71</sub>BM blends investigated (Fig. 1a and Table 1).<sup>27</sup> However, for fullerene-based blend systems, there is limited potential to further enhance the  $V_{oc}$  value since the energy level of the fullerene acceptor cannot easily be adjusted and only the energy level of the polymer donor can be tuned. Nonfullerene acceptors (NFAs), on the other hand, offer more opportunities to deliver higher  $V_{oc}$  due to more adjustable properties of both the donor and acceptor. For example, based on the PBDB-TF polymer donor, Cui *et al.* found

Table 1 The photovoltaic parameters of devices with different polymer:PC<sub>71</sub>BM blend systems under 1 sun and 1000 lx LED luminance. Adapted from ref. 27 with permission from WILEY-VCH

Device	Light source	$V_{oc}$ (V)	$J_{sc}$ (1 sun: mA cm <sup>-2</sup> ) (LED: $\mu$ A cm <sup>-2</sup> )	FF (%)	$P_{out}$ (mW cm <sup>-2</sup> )	PCE (%)
PDTBTBz-2F <sub>anti</sub> :PC <sub>71</sub> BM (device A)	1 sun	0.903	14.4	53.3	6.93	6.9
	LED	0.817	112.4	70.4	0.065	23.1
P3HT:PC <sub>71</sub> BM (device B)	1 sun	0.600	9.3	47.3	2.64	2.6
	LED	0.498	73.7	71.9	0.026	9.4
PBDB-T:PC <sub>71</sub> BM (device C)	1 sun	0.764	11.8	67.2	6.06	6.0
	LED	0.669	90.2	71.3	0.043	15.3
PTB7:PC <sub>71</sub> BM (device D)	1 sun	0.670	13.6	67.4	6.14	6.1
	LED	0.569	87.6	69.3	0.035	12.3



**Table 2** The photovoltaic parameters of the devices with different PBDB-TF:acceptors under 1 sun and 1000 lx LED illumination. Adapted from ref. 28 with permission from WILEY-VCH

Device	Light source	$V_{oc}$ (V)	$J_{sc}$ (1 sun: mA cm <sup>-2</sup> ) (LED: $\mu$ A cm <sup>-2</sup> )	FF (%)	$P_{out}$ (mW cm <sup>-2</sup> )	PCE (%)
PBDB-TF:PC <sub>71</sub> BM	1 sun	0.945	12.9	67.1	8.43	8.43
	LED	0.784	94.1	74.1	0.0547	18.1
PBDB-TF:ITCC	1 sun	1.10	14.3	64.3	10.3	10.3
	LED	0.962	95.8	72.2	0.0665	22.0
PBDB-TF:IT-4F	1 sun	0.872	20.1	68.7	12.2	12.2
	LED	0.712	113.0	78.0	0.0628	20.8

that the ITCC acceptor, which has a higher effective bandgap (1.69 eV) than IT-4F (1.31 eV), results in higher  $V_{oc}$  under both AM 1.5G illumination (1.1 V vs. 0.872 V) and indoor light conditions (0.962 V vs. 0.712 V at 1000 lx LED light) (Fig. 1b and Table 2).<sup>28</sup> In addition to a higher effective bandgap, reducing energy loss ( $E_{loss}$ ) is also an important consideration. Cui *et al.* synthesised a wider-gap NFA molecule IO-4Cl with a smaller  $E_{loss}$  of 0.6 eV in blend with PBDB-TF under AM 1.5 G illumination, compared to a PBDB-TF:ITCC blend which has a  $E_{loss}$  of 0.65 eV. As a result, the PBDB-TF:IO-4Cl cell exhibits a higher  $V_{oc}$  of 1.1 V under 1000 lx LED light compared with the 0.962 V for the PBDB-TF:ITCC cell.<sup>17</sup>

A wide gap close to 1.9 eV (ideal bandgap) is beneficial for matching the absorption spectrum with the indoor light sources and therefore obtaining superior photovoltaic performance,<sup>29</sup> while the majority of the photoactive materials used in the indoor OPVs reported so far have a bandgap narrower than the optimal value. The above-mentioned PBDB-TF:ITCC and PBDB-TF:IO-4Cl blends with a decent bandgap and well-match absorption spectrum have demonstrated outstanding PCEs of 22.0% and 26.1% under 1000 lx LED illumination, respectively.<sup>17,28</sup> Ding *et al.* recently reported an efficient all-polymer blend system with a bandgap over 1.9 eV, which is promising for indoor applications. The authors introduced a new class of polymer acceptors containing boron–nitrogen coordination bonds (B ← N), which possess suitable bandgaps with tuneable LUMO and HOMO energy levels.<sup>30</sup> In particular, the polymer acceptor PBN-10 (which has a bandgap of 1.95 eV) in blend with the polymer donor CD1 (which has a bandgap of 1.93 eV) as the active layer exhibits a PCE of 26.2% under FL illumination at 1000 lx with a high  $V_{oc}$  value of 1.14 V (Fig. 1c and Table 3). The high device performance of the new target-developed wide-gap materials illustrates the great potential of OPV devices for further performance enhancement under low light conditions.

It was recently reported that the performance of OPVs under low light conditions can be improved through morphology optimisation of the active layer. Lee *et al.* found that the performance of a small molecular donor-based OPV system (BTR:PCBM) under low light can be improved by balancing the crystallisation and the phase separation of the active layer *via* solvent vapour annealing (SVA), obtaining an outstanding PCE (~28%) among the fullerene based OPV devices under 1000 lx.<sup>31</sup> In addition, the choice of transporting layers is also found to be crucial for achieving high-performance indoor OPVs. Ma *et al.* reported a high-efficiency indoor OPV device based on a polymer:nonfullerene system PM6:Y6-O with a band-aligned electron transporting interlayer (ETL) PDI-NO, which has a deep HOMO energy level with good hole-blocking properties. A high PCE of 30.1% was obtained with a high FF of 76% due to low leakage current and trap-assisted recombination in PDI-NO-based OPVs under 1650 lx LED illumination.<sup>9</sup> Furthermore, OPVs based on ternary or quaternary blend systems are also a promising route for high-performing indoor PV applications.<sup>32</sup> For example, by introducing a polymer donor PDTSTPD to a binary PCDTBT:PC<sub>71</sub>BM blend system, the efficiency is increased from 16.5% to 20.8% under 300 lx fluorescence light.<sup>33</sup> This is due to the passivating effect of the PDTSTPD component on the shallow traps near the PCDTBT:PC<sub>71</sub>BM band edge, facilitating an enhanced hole mobility. Recently, Cho *et al.* introduced a third component Y-Th2 acceptor into a host PM6:Y6 nonfullerene blend system, achieving a PM6:Y-Th2:Y6-based ternary OPV device with a high PCE of up to 22.72% under LED light at 1000 lx. The addition of NFA Y-Th2 was found to broaden the absorption in visible light, adjust the energy level alignment between donor and acceptor and optimise the blend compatibility, allowing efficient charge-carrier transport in the active layer.<sup>34</sup> Moreover, a quaternary OPV (Q-OPV) blend system comprising two polymer donors and two small molecule acceptors was demonstrated by Nam *et al.*<sup>35</sup>

**Table 3** The photovoltaic parameters of the OPVs based on CD1:PBN-10 and CD1:ITIC blend films under 1sun and under 1000 lx FL luminance. Adapted from ref. 30 with permission from The Royal Society of Chemistry

Device	Light source	$V_{oc}$ (V)	$J_{sc}$ (1 sun: mA cm <sup>-2</sup> ) (LED: $\mu$ A cm <sup>-2</sup> )	FF (%)	$P_{out}$ (mW cm <sup>-2</sup> )	PCE (%)
CD1:PBN-10	1 sun	1.29	10.10	60.8	7.93	7.93
	FL	1.14	120	66.2	0.091	26.2
CD1-ITIC	1 sun	0.91	16.39	58.3	8.69	8.69
	FL	0.78	116	68.1	0.062	17.9



Compared to the reference binary OPV system, this Q-OPV system has advantages of improved charge transfer processes from the donors to acceptors, increased  $R_{sh}$  and  $V_{oc}$  values and well-aligned energy levels of the donors and acceptors. It was further found that higher  $R_{sh}$  can be achieved in thicker Q-OPV devices, resulting in increased FF and  $J_{sc}$  and thereby enhanced PCE with increasing the active layer thickness. Q-OPVs are also promising for semi-transparent and large area applications due to their high tolerance to variations in active layer thickness, which will be discussed further below.

In summary, high-performance indoor OPVs can be achieved by (a) optimising the bandgap of donors and acceptors to match the emission spectra of indoor light sources, thereby ensuring efficient light absorption; (b) targeting blend systems with a high  $V_{oc}$  in conjunction with a low ideality factor; (c) targeting materials and device designs with sufficiently large shunt resistance and a low dark current; (d) optimising the materials and device processing conditions including the blend morphology and interlayers and (e) adopting suitable ternary/quaternary blend systems.

**2.1.2 Large area devices.** A high tolerance to the variations in the device active layer thickness is desirable for the development of high-performance large-area OPVs, since the large-scale processing through, *e.g.*, printing, blade coating, and spray coating may induce inhomogeneity across the OPV film.

With an increased device active area and active layer thickness,  $R_s$  typically increases significantly, thereby limiting the device performance under high light conditions. However, such an increase in  $R_s$  may not be a key consideration for indoor OPVs owing to the negligible effect of  $R_s$  on their performance under low light conditions, making it possible to achieve superior device performance under low light with large active areas and high device thicknesses. Yin *et al.* demonstrated an OPV system based on a porphyrin-based polymer P1 whose efficiency under low light is relatively invariant on the active layer thickness, showing a similar PCE within the range of 18.4% to 19.1% under 300 lx LED light when the active layer thickness is increased from 100 nm to 200 nm.<sup>36</sup> Shin *et al.* systematically investigated the thickness dependence of PPDT2FBT:PC<sub>70</sub>BM-based OPVs under low light conditions with varying active layer thicknesses from 120 nm to 870 nm.<sup>37</sup> It was found that when the thickness of the photoactive layer is larger than 280 nm, the  $R_s/R_{sh}$  ratio becomes very low ( $<0.007$ ), resulting in a negligible decrease in both FF and  $J_{sc}$  under LED illumination at 1000 lx even when the active layer thickness is increased to 870 nm. They conclude that the large  $R_{sh}$  value resulting from the high photoactive thickness, in conjunction with the excellent spectrum match between the active layer absorbance and indoor light sources, is critical to achieve efficient indoor OPV devices with a high  $J_{sc}$  and FF. Cui *et al.* fabricated a large area



Fig. 2 (a) J–V characteristics of an OPV device with a 4.0 cm<sup>2</sup>-large area under 1 sun and an LED illumination. Inset: a photograph of the 4 cm<sup>2</sup> device. Reproduced with ref. 17 with permission from Springer Nature. (b) J–V characteristics of an 8-pixel module OPV device (red) with a total active area of 100 cm<sup>2</sup> and a pixel (purple), respectively under FL at 300 lx. Inset: a photograph taken of this module. Reproduced with ref. 23 with permission from AIP Publishing. (c) Photographs, schematic and (d) J–V characteristics of 6 series-connected devices fabricated on a glass substrate and a flexible substrate. Reproduced with ref. 38 with permission from the American Chemical Society.



OPV device (4 cm<sup>2</sup>) with an active layer thickness of ~200 nm based on the PBDB-TF:IO-4Cl blend system by blade-coating (Fig. 2a).<sup>17</sup> A high PCE of 23.9% was obtained under 1000 lx LED light, in conjunction with a much higher FF value (75.3%) than that obtained under high light conditions (55.9% under 1 sun) due to reduced non-geminate recombination.

To further explore the potential of indoor OPVs toward future commercialisation, Lee *et al.* fabricated an 8-pixel module with an active area of 100 cm<sup>2</sup> by spin-coating PCDTBT:PC<sub>71</sub>BM solution on a 14 cm × 14 cm substrate, generating a maximum power of 938 μW under FL at 300 lx (Fig. 2b).<sup>23,24</sup> Arai *et al.* fabricated OPV modules with a total active area of 9.5 cm<sup>2</sup> by connecting 6 cells in series based on the BDT-1T-ID:PNP blend system, obtaining a PCE of 15% with an output power of 111 μW cm<sup>-2</sup> under 200 lx white LED light. Modules were also prepared on a flexible PEN substrate, showing a power output of 101 μW cm<sup>-2</sup> under the same low light conditions.<sup>38,39</sup> The authors further fabricated OPV modules based on the 1DTP-ID:PNP blend systems with a total active area of 9.6 cm<sup>2</sup> on flexible PEN substrates, obtaining a flexible and large-area OPV device with a PCE of 17% under 200 lx LED light (Fig. 2c).<sup>26</sup> These studies demonstrate the unique advantages of OPVs as a promising candidate for indoor PV applications with highly adjustable materials properties (*e.g.* colour, optical transparency) and device form factor (*e.g.* size, shape, flexibility), with outstanding potential for integration with a broad range of target applications.

**2.1.3 Semi-transparent and flexible OPV devices.** Although outstanding low-light performance has been obtained for lab-scale OPV devices based on various blend systems, the majority of such devices have been fabricated and optimised without considering the optical transmittance of the device layers. For certain applications (*e.g.* PV integrated on windows), a balance between the power generation and optical transparency, namely semi-transparent indoor OPV devices may be required, imposing an additional requirement for high optical transmittance in the visible region of the device active layer, interlayers and electrodes.

A common strategy to achieve efficient semi-transparent OPVs under 1 sun illumination is to use a thin active layer film with near-infrared (NIR) absorbers to allow higher transmission in the visible light region.<sup>40</sup> This strategy, however, is not suitable for indoor OPVs since the majority of indoor light sources nowadays are energy efficient and mainly emit in the visible region, thereby resulting in limited light absorbance and low PCE. To overcome the challenge, Yin *et al.* introduced a porphyrin-based donor P2, the absorbance of which has a valley in the region most sensitive to human eyes but with stronger absorption at the blue/red end, allowing high visible light transmittance and good colour rendering under indoor cold light sources. A semi-transparent P2:PC<sub>71</sub>BM OPV device was fabricated with an active layer thickness of 70–80 nm, showing a PCE of 10.7% under a LED illumination of 300 lx with an average visible transmittance (AVT) of 67% of the active layer.<sup>41</sup> Nam *et al.* fabricated a semi-transparent quaternary OPV device with a whole device AVT of 13.7% by only reducing the thickness of Ag to 15 nm, whose active layer thickness is

170 nm, with an AVT of 48.3%. This semi-transparent OPV device had achieved a PCE of 14.64% under LED with 1000 lx (Fig. 3a).<sup>35</sup>

The development of devices with high optical transmittance and mechanical flexibility is also an important consideration for indoor OPVs. An OPV device with a ZnO/Ag/ZnO (ZAZ) transparent bottom electrode was recently introduced by Lee *et al.*<sup>42</sup> ZAZ electrode-based OPVs achieved transmittances up to 92% in the visible region and a sheet resistivity of 4.8 Ω sq<sup>-1</sup>, yielding a PCE of 12.3% under a LED lamp at 500 lx. The authors further fabricated a flexible OPV device with a ZAZ electrode, obtaining a PCE of 10.2% under a LED lamp at 500 lx with fairly good mechanical stability (with PCE dropping from 10.2% to 8% upon 400 cycling bends, Fig. 3b).

## 2.2 PPVs for indoor application

PPV cells have been one of the hottest topics in solar cells in recent years, achieving a record PCE over 25% for single-junction devices under standard solar irradiation, owing to the outstanding optoelectronic properties of perovskite semiconductors including strong optical absorption, high carrier mobility and lifetimes, and high tolerance to defects.<sup>43,44</sup> The application of PPVs in low light applications was first reported by Chen *et al.*<sup>45</sup> with an inverted device structure of PEDOT:PSS/MAPbI<sub>3</sub>/PCBM/TmPyPB/Ag, achieving a PCE of 27.4% for small area (5.1 mm<sup>2</sup>) devices and 20.4% for large area (5.44 cm<sup>2</sup>) devices under 1000 lx FL illumination, with promising long-term stability (maintained 97% of initial efficiency after 40 days under ambient indoor lighting with device encapsulation). Since then, the PCE of PPV devices under indoor light has been improved substantially, primarily driven by further optimisation of the fabrication process (in particular through engineering of the perovskite layer composition and interlayers) to achieve optimal control of the perovskite crystallinity, trap states and carrier dynamics. The recent progress on materials development and device engineering methods of PPVs for indoor applications is summarised in the following section.

**2.2.1 Performance improvement methods.** Perovskite PV materials are composed of a set of material compounds with an ABX<sub>3</sub> crystal structure, where A is a large monovalent cation, B is a much smaller divalent cation, and X is usually a halide anion that bonds to A and B cations. The ability of elements A, B, and X to form a perovskite structure can be predicted by using the ionic-radius related Goldschmidt tolerance factor *t* and octahedral factor *μ*, which should be in the range of 0.8 < *t* < 1.0 and 0.442 < *μ* < 0.895 in order to form a stable ABX<sub>3</sub> structure.<sup>46,47</sup> The tolerance of *t* and *μ* allows a wide selection of A, B and X elements to further tune the perovskite's structural, energetic and optoelectronic properties. Therefore, compositional engineering can be an attractive strategy to adjust the bandgap of the perovskite materials in order to achieve the optimal value ~1.9 eV, thereby enhancing device performance under low light.<sup>45,48</sup> In recent years, the most common perovskite materials for indoor applications are methyl ammonium lead iodide CH<sub>3</sub>NH<sub>3</sub>PbI<sub>3</sub> (MAPbI<sub>3</sub>) and its triple-cation tailored structures, with a bandgap of ~1.6 eV.<sup>49</sup> Although this value is lower than



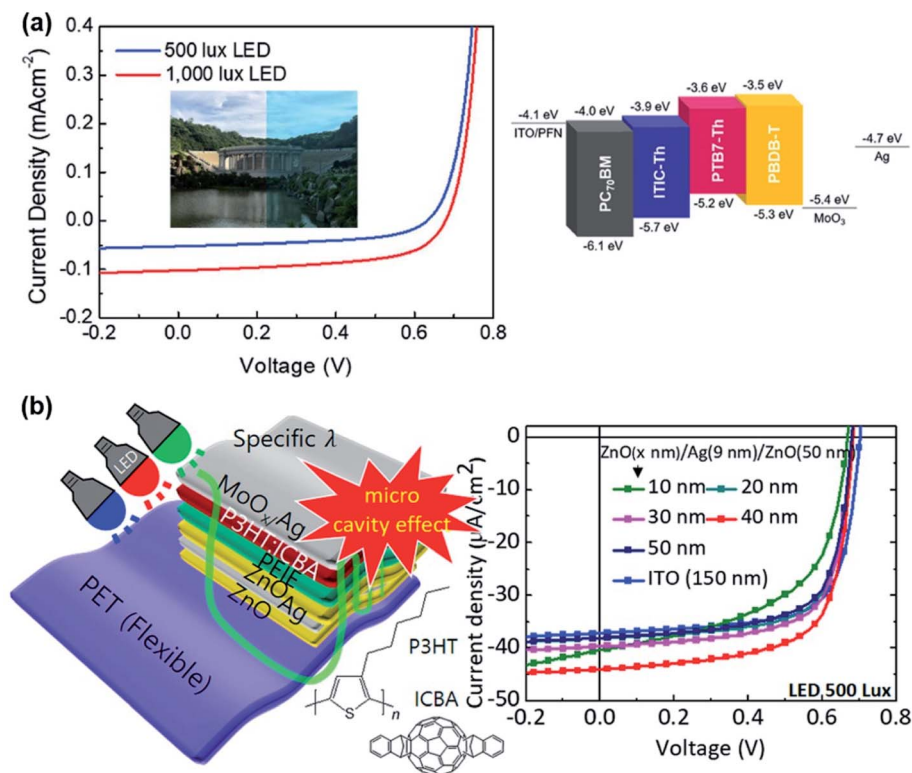


Fig. 3 (a)  $J$ - $V$  characteristics of a quaternary-OPV device under a LED illumination, and energy level alignment of the quaternary OPV device. Inset: a photograph taken with (right) and without (left) a quaternary OPV filter. Inset: a photograph taken with (right) and without (left) a quaternary OPV device. Reproduced from ref. 35 with permission from WILEY-VCH. (b) Schematic illustration and  $J$ - $V$  characteristics of a flexible OPV structure with the ZnO-Ag-ZnO transparent electrode under indoor light illumination. Reproduced with ref. 42 with permission from Elsevier.

the ideal bandgap of 1.9 eV, the devices still exhibit decent performances with a  $V_{oc}$  of up to 1.1 V due to a high external quantum efficiency (EQE) within the visible region and a small voltage loss.<sup>1</sup> There is also some research effort in further adjusting the bandgap of PPVs through halide engineering in order to achieve higher device performance under low light. While mixed halides can often have a detrimental effect upon phase segregation,<sup>50</sup> such an effect can be effectively mitigated through delicate halide component tailoring. For example, it is found that both  $Br^-$  and  $Cl^-$  tuned PPV devices exhibit higher  $V_{oc}$  and overall better PCE than the  $MAPbI_3$  based PPVs under 1000 lx FL light (Fig. 4a and b).<sup>51</sup> With simultaneous tuning of the  $I^-/Br^-/Cl^-$  composition, a wide bandgap of 1.8 eV was achieved with minimal influence on phase segregation, resulting in a PCE of over 36% under 1000 lx FL light.<sup>51</sup> Lim *et al.* obtained an outstanding PCE of over 34% under 1000 lx LED light by only optimising the Br doping level in perovskite  $MAPbI_{3-x}Br_x$ , which exhibits a tunable bandgap in the range of 1.58 eV to 1.73 eV, enlarged grain size and reduced surface defects.<sup>52</sup>

In addition to bandgap optimisation, good film crystallinity and low defect density are also important considerations for PPVs in order to achieve efficient charge transport with long electron and hole-diffusion lengths. In particular, trap states could dominate PV performance under low light conditions, since there are not enough photocarriers to fill these traps,

leading to inefficient charge separation at the interfaces and perovskite grain boundaries as well as high leakage current.<sup>53</sup> Therefore, current strategies for performance enhancement of PPVs under low light have been mainly focused on compositional engineering in order to reduce the defect density of the perovskite materials, and through interfacial engineering in order to suppress the leakage current and improve the charge extraction at the interfaces.<sup>51,53,54</sup>

Dagar *et al.* used a  $SnO_2/MgO$  double ETL in the PPV device to rectify the dark  $J$ - $V$  curves by effectively reducing the number of pin holes and blocking the perovskite-electrode contact.<sup>55</sup> A PCE of 26.9% under 400 lx LED illumination was achieved, representing a 20% enhancement compared to the device only employing a  $SnO_2$  layer. Lee *et al.* reported significantly improved performances of PPVs under 1000 lx FL light after replacing PTAA HTL with spiro-OMeTAD in a conventional device structure (resulting in an increased  $P_{max}$  from 16.1 to 115.6  $mW\ cm^{-2}$ ) and replacing PEDOT:PSS HTL with poly-TPD in an inverted device structure (resulting in an increased  $P_{max}$  from 68 to 111.9  $mW\ cm^{-2}$ ), which is attributed to the significantly suppressed dark current.<sup>56</sup> Li *et al.* employed 1-butyl-3-methylimidazolium tetrafluoroborate ( $[BMIM]BF_4$ ) as the modification layer to passivate the surface trap-states of  $PC_{61}BM/Ag$  and achieved a PCE of 35.2% under a 1000 lx fluorescent lamp (see Fig. 4c and d).<sup>57</sup> Noh *et al.* reported a  $SnO_2/ZnO$  bilayer-structured ETL, which not only possesses suitable







Fig. 4 (a)  $J$ - $V$  curves of the three groups of halide-engineered devices under 1000 lx FL light; inset shows the PPV device ( $1.5 \times 1.5 \text{ cm}^2$ ) and the test holder for  $0.1 \text{ cm}^2$  active area.<sup>51</sup> (b) SEM cross-sectional views of  $\text{MAPbI}_2\text{Br}$  and  $\text{MAPbI}_{2-x}\text{BrCl}_x$  films.<sup>51</sup> Reproduced with permission ref. 51. Copyright 2019, WILEY-VCH. (c)  $J$ - $V$  curves of PPV based on PCBM, PCBM/BCP, PCBM/[BMIM]BF<sub>4</sub> ETLs under 1000 lx; inset shows the device picture.<sup>57</sup> (d) SEM cross-sectional views of [BMIM]BF<sub>4</sub>-based PPV layers.<sup>57</sup> Reproduced with permission ref. 57. Copyright 2019, WILEY-VCH.

energy band matching but also suppressed trap-assisted recombination at the  $\text{MAPbI}_3$  interface, realising a PCE of up to 37.2% under 1000 lx LED light.<sup>10</sup> It was found that further optimisation of the fabrication process of PPV devices can also reduce the trap density at the perovskite/ETL or perovskite/hole transporting layer (HTL) interfaces. For example, PPV devices prepared with an atomic-layer-deposited compact  $\text{TiO}_2$  (c- $\text{TiO}_2$ ) interlayer between the ITO and mesoporous  $\text{TiO}_2$  (m- $\text{TiO}_2$ ) layers exhibit a decreased number of pin holes, resulting in improved device performance under both indoor and outdoor illumination conditions compared to devices employing  $\text{TiO}_2$  interlayers deposited by sol-gel spin coating and spray pyrolysis.<sup>58</sup> A PPV device employing a two-step processed PCBM layer, where a thin diluted PCBM layer was first deposited to fill the traps of the perovskite films formed during the thermal annealing process, followed by a thick PCBM layer deposited on the diluted PCBM layer, was found to exhibit better performance than a device employing one-step processed PCBM ETLs.<sup>45</sup>

In summary, high-performance indoor PPV devices can be facilitated by careful compositional engineering to adjust the material bandgap to  $\sim 1.9 \text{ eV}$ , as well as optimisation of the materials and device processing routes and interfaces to achieve good perovskite crystallinity with a low density of defects.

**2.2.2 Flexible PPV devices.** Flexible PPVs have been investigated in recent years and PCEs as high as 19.11% under 1 sun have been obtained<sup>59,60</sup> with the development of flexible

substrates and optimisation of perovskite materials.<sup>61,62</sup> In order for flexible PPVs to be applied under indoor conditions, several key challenges need to be addressed, including, in particular, the formation of bend-induced pin holes and cracks in the device layers (leading to high leak current) and the requirement for low-temperature processing for device fabrication ( $<150 \text{ }^\circ\text{C}$  for polyethylene terephthalate-PET substrates) without compromising device performance. It has been demonstrated that employing a thick c- $\text{TiO}_2$  blocking layer at the ITO/ETL interface can effectively decrease the number of pin-holes, thereby achieving superior device mechanical stability.<sup>63</sup> The c- $\text{TiO}_2$  and m- $\text{TiO}_2$  based device structures of PET/ITO/c- $\text{TiO}_2$ /m- $\text{TiO}_2$ / $\text{MAPI}_{3-x}\text{Cl}_x$ /spiro-MeOTAD/Au showed a PCE of 12.1% under a 400 lx white LED lamp and can maintain this efficiency after 100 consecutive bending cycles with a bending radius of 14 mm. Based on this, Dagar *et al.* further optimised the device structure by replacing c- $\text{TiO}_2$  with solution-processed  $\text{SnO}_2$ , and the resulting device was able to work efficiently after 100 consecutive bending cycles with a radius of curvature  $\geq 20 \text{ mm}$ , retaining 80% of its initial PCE (13.3% under 400 lx white LED light).<sup>64</sup> Nevertheless, the performance of flexible PPVs is currently much lower than that of their rigid glass-based counterparts (*e.g.* a PCE of 24% can be achieved employing the same PPV device structure on glass under 400 lx white LED light), primarily owing to the modest endurance of PET substrates to elevated processing temperatures. For example, the ITO electrode can only be deposited on



PET substrates at a maximum temperature of  $\sim 150$  °C, under which ITO cannot form uniform grains leading to lower transmittance and higher resistivity,<sup>65</sup> while a temperature range of 160–310 °C is required for the deposition of high-quality ITO electrode. To address this problem, Hermosa *et al.* developed a conductive ultra-thin flexible glass (FG) with high-temperature compatibility (700 °C) as a promising alternative to PET.<sup>66</sup> The ITO coated FG showed notable transmittance  $>80\%$ , a sheet resistance of  $13 \Omega$  per square and bendability surpassing 1600 bending cycles at 20.5 mm curvature. The resulting PPV cells delivered PCEs of  $>22\%$  under 400 lx LED illumination based on the device structure of FG/ITO/SnO<sub>2</sub>/m-TiO<sub>2</sub>/MAPbI<sub>3</sub>/spiro-OMeTAD/Au (see *J-V* curve in Fig. 5a). Lim *et al.* demonstrate the feasibility in the use of flexible PPVs as the power supply for low-power electronics by connecting a flexible mixed-halide [(MAPbI<sub>3</sub>)<sub>0.95</sub>(FAPbBr<sub>2</sub>)<sub>0.05</sub>] device to a solar-powered motor. Under 1000 lx white LED illumination (colour temperature = 6400 K), this PPV device (active area =  $0.12 \text{ cm}^2$ ) generated comparable maximum power densities of  $0.181$  and  $0.175 \text{ mW cm}^{-2}$  in the flat and bent status respectively (see Fig. 5b). In order to power the motor which requires a power output  $>0.8 \text{ mW cm}^{-2}$ , a larger PPV device with an active area of  $0.48 \text{ cm}^2$  was fabricated and the illumination was increased to 5000 lx, under which the device can generate a maximum power density of  $0.846 \text{ mW cm}^{-2}$  and PCE of 28.63% as shown in Fig. 5c. During the continuous bending of the device, the motor operated stably without any reduction in the rotational speed.<sup>67</sup>

**2.2.3 Large scale devices/modules.** The most efficient PPVs developed to date have typically been fabricated on small-area devices ( $\sim 0.1 \text{ cm}^2$ ). To integrate PPV cells into electronic products and generate enough power, large-area devices ( $\sim 1 \text{ cm}^2$ ) and modules ( $\sim 10 \text{ cm}^2$ ) need to be fabricated, with several efficient large-area indoor PPVs successfully demonstrated to date. For example, it has recently been demonstrated that the halide-engineered perovskite MAPbI<sub>2-x</sub>BrCl<sub>x</sub> PPVs are not only able to achieve an extraordinary PCE of 36.2% on small devices ( $0.1 \text{ cm}^2$ ) but also a PCE of over 30% with a larger active area of  $2.25 \text{ cm}^2$  under 1000 lx fluorescent light with a device architecture of ITO/NiO<sub>x</sub>/MAPbI<sub>2-x</sub>BrCl<sub>x</sub>/PCBM/BCP/Ag (Fig. 5d).<sup>51</sup> The [BMIM]BF<sub>4</sub> ETL interlayer modified MAPbI<sub>3</sub> PPV device exhibits a high PCE of 23.16% under 1000 lx FL light with an active area of  $4 \text{ cm}^2$  in conjunction with reduced interfacial traps and defects.<sup>57</sup> Lee *et al.* fabricated a mini-module (with five subcells connected in series and a total active area of  $5 \times 5 \text{ cm}^2$ ) with a device architecture of consecutive stacks of m-TiO<sub>2</sub>, m-ZrO<sub>2</sub> and carbon on FTO substrates.<sup>56</sup> The resulting PPVs showed a promising maximum power density ( $P_{\text{max}}$ ) of  $16.3$  and  $89.4 \mu\text{W cm}^{-2}$  under 200 and 1000 lx FL lamps respectively.

For the fabrication of larger modules, more processing problems should be considered. A key consideration is to achieve high film uniformity over large-area substrates without pinholes or other inhomogeneity during the precursor solution drying and perovskite crystallisation processes. However, the crystallisation kinetics of perovskites are different on small and

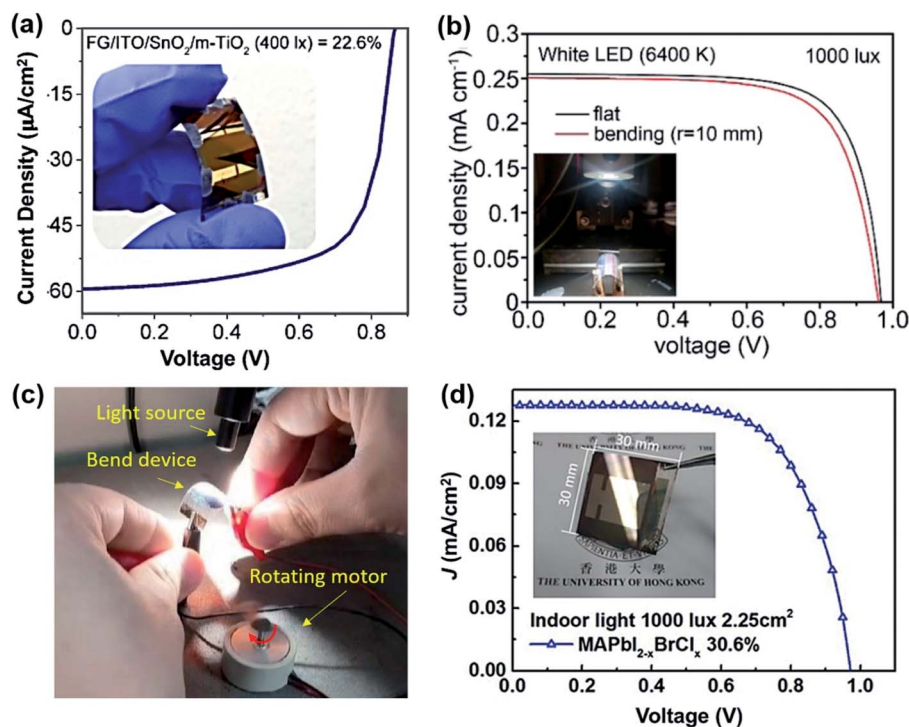


Fig. 5 (a) *J-V* curve of the FG based device under 400 lx LED illumination; inset shows the photograph of a curved FG-PPV device. Adapted with permission ref. 66 under the CC BY-NC-ND license. (b) *J-V* curves of the flat and bent devices at a radius of 10 mm and the photo of the testing platform (inset).<sup>67</sup> (c) Photo of the simulated experiment at 5000 lx for the flexible PPV device interconnected to the motor.<sup>67</sup> Adapted from ref. 67 with permission from the American Chemical Society. (d) *J-V* curve of the MAPbI<sub>2-x</sub>BrCl<sub>x</sub> base PPV device under 1000 lx FL light with a large area of  $3 \times 3 \text{ cm}^2$  and active layer of  $2.25 \text{ cm}^2$ . Reproduced with permission ref. 51. Copyright 2019, WILEY-VCH.



large area substrates, leading to multidirectional crystal growth of the precursor on a large-area substrate without control.<sup>68</sup> To solve this problem, several approaches have been proposed, such as using anti-solvents to extract the solvents from the precursor solution and accelerate perovskite precipitation, expanding the precursor processing window (the time needed for perovskite material precipitation) by selecting mixed solvents with longer evaporation times and using chemical additives to control crystal growth.<sup>68–70</sup> A  $10 \times 10 \text{ cm}^2$  PPV module with a PCE of close to 18% has recently been demonstrated through the dynamic anti-solvent process.<sup>71</sup> In addition, for large modules, inhomogeneity of the layer thickness across the substrate will affect the current and FF of the sub cells with the worst sub cell dictating the overall current and FF in the series-connected modules, which needs to be optimised delicately to ensure consistent distribution of each layer's thickness. With such optimisation, Rossi *et al.* manufactured a stable A4-size module (with an active area of  $198 \text{ cm}^2$ ) with PCE  $\sim 6.6\%$  under 1 sun and an outstanding PCE of  $\sim 18\%$  under 1000 lx FL lighting.<sup>72</sup>

### 2.3 QDPVs for indoor application

QDs have been brought to the forefront of the development of high-definition television (HDTV) over the past 2–3 years as a more versatile alternative to organic LEDs with a higher colour gamut. As an immediately related technology, the development

of QDPVs can directly benefit from QD LEDs as a highly promising PV technology<sup>73,74</sup> that suffer no compromise between high theoretical efficiency, stability and low cost, showing excellent ambient tolerance after QD surface passivation and band alignment.<sup>75,76</sup> Compared with perovskites, conventional bulk semiconductors and organic semiconductors, QDs possess a low photon energy threshold for multiple exciton generation, which enables QDPVs to go beyond the Shockley–Queisser (SQ) limit.<sup>77,78</sup> For free-standing QDs or colloidal dispersion, due to the spatial confinement of the QDs, electron–hole pairs interact strongly through the Coulomb potential, which enables electron–hole pairs to remain as excitons, not free-carriers; furthermore, free carriers can only form upon dissociation of the excitons.<sup>79</sup> QDs can enhance the efficiency of the electron–hole pair multiplication processes where the excess photon energy can be used to produce additional electron–hole pairs, instead of loss as dissipated heat.<sup>80</sup> Meanwhile, the highly tunable bandgap of QDs facilitates efficient energy harvesting in the near to short-wave infrared region of the solar spectrum.<sup>81</sup> However, the current QDPV 1 Sun efficiency is still lower than those of OPVs and perovskite solar cells which is mainly due to the complicated material synthesis process and a vast number of defect states generated during device fabrication. While QDPVs usually exhibit only modest PCE (around 13%)<sup>82,83</sup> compared to OPVs and PPVs under 1 sun condition, they have strong potential in achieving high device performance under low light conditions, considering the highly

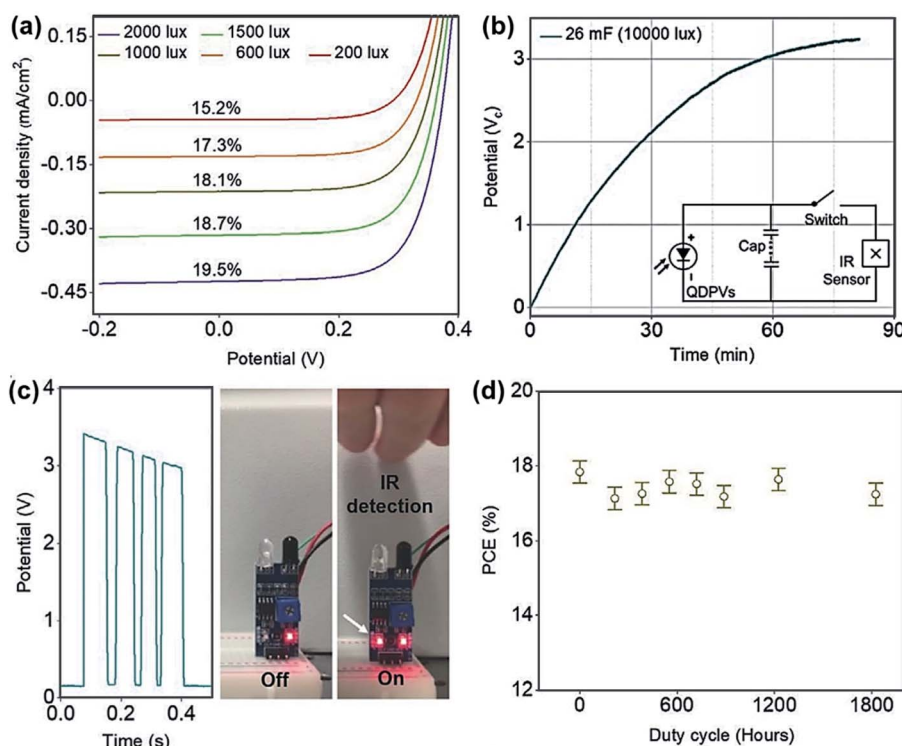


Fig. 6 (a)  $J$ – $V$  curves and PCE values of the QDPVs at different room light irradiance levels. (b) Capacitor charging curve under 10 000 lx light. Inset describes an integrated circuit of QDPVs, capacitors and an IR sensor. (c) Snapshots and transient signals from the IR sensor. (d) The unencapsulated QDPV PCE stability performance under 1000 lx insulation for a continuous 1800 h exposure. Reproduced from ref. 11 with permission from WILEY-VCH.



tunable bandgaps of QDs by changing their size,<sup>84,85</sup> making them an efficient low light energy harvester.

To investigate the potential of QDPVs for indoor applications, Hou *et al.* demonstrated the first indoor QDPV device based on lead sulfide (PbS) quantum dots.<sup>11</sup> The results show that a maximum PCE of 19.5% can be achieved under FL illumination from 200 lx to 2000 lx (see Fig. 6a), significantly higher than the record PCE of QDPVs under 1 sun ( $\sim 13.8\%$ ).<sup>82</sup> The authors further demonstrated the feasibility of QDPVs in powering indoor-light-sensor networks. As shown in Fig. 6b, the QDPV matrix can readily charge the integrated capacitor (inset) under 10 000 lx, under which the infrared sensor can work successfully as indicated by the dynamically tracked sensor process (Fig. 6c). To investigate the stability of QDPVs under typical indoor operating environments, the evolution of their device performance under continuous low light exposure (1000 lx insolation) in the ambient atmosphere without encapsulation was recorded. As shown in Fig. 6d, minimal degradation in the device performance of QDPVs was observed upon 1800 hours of continuous light exposure. The practical application and long lifetimes demonstrated in the work of Hou *et al.* are credible evidence of the high commercialisation potential of indoor QDPVs.

It should be noted that the studies on QDPVs for low light applications are still limited in the literature. While the outstanding low light performance of QDPVs achieved in the work above is a good demonstration of the potential of indoor QDPVs, further investigations are urgently needed in order to optimise the device performance *via* QD materials and size engineering. Nevertheless, given the successful commercialisation of QD based HDTV as well as the fast development of QD ambient lighting, QDPVs should be considered a competitive candidate for future indoor PV applications. In particular, since there is no scientific barrier between the red QD LEDs and QDPVs, the established LED device processing technologies and the excellent compatibility of QDs with flexible, large area and transparent electrodes, are expected to be easily implemented for indoor QDPVs. In addition, QD thermophotovoltaic devices can be alternative promising candidates for harvesting indoor energy into electrical power by utilising a small bandgap semiconductor that absorbs the low-energy infrared photons from radiated thermal energy and using asymmetric contacts to the absorber (such as QD layers) to transfer net electrical power to load.<sup>86</sup>

To compare the optimal bandgap for outdoor and indoor PVs as well as the state-of-the-art of different indoor PV technologies, a plot of the SQ-limited PCE as a function of optical bandgap, as well as plots of device PCE and  $P_{\max}$  as a function of bandgap and illuminance, is shown in Fig. 7, with the device parameters of several representative outstanding PV cells summarised in Table 4. Fig. 7a exhibits an optimal bandgap of  $\sim 1.9$  eV for indoor PV under typical indoor light sources, in comparison to the range of 1.1 to 1.4 eV under AM 1.5 G condition.<sup>87</sup> Fig. 7b and c show that a larger energy bandgap closer to 1.9 eV can result in a higher device PCE and  $P_{\max}$  for OPVs, PPVs and QDPVs under low light, with indoor PPVs currently exhibiting the highest PCE and  $P_{\max}$ . It should be

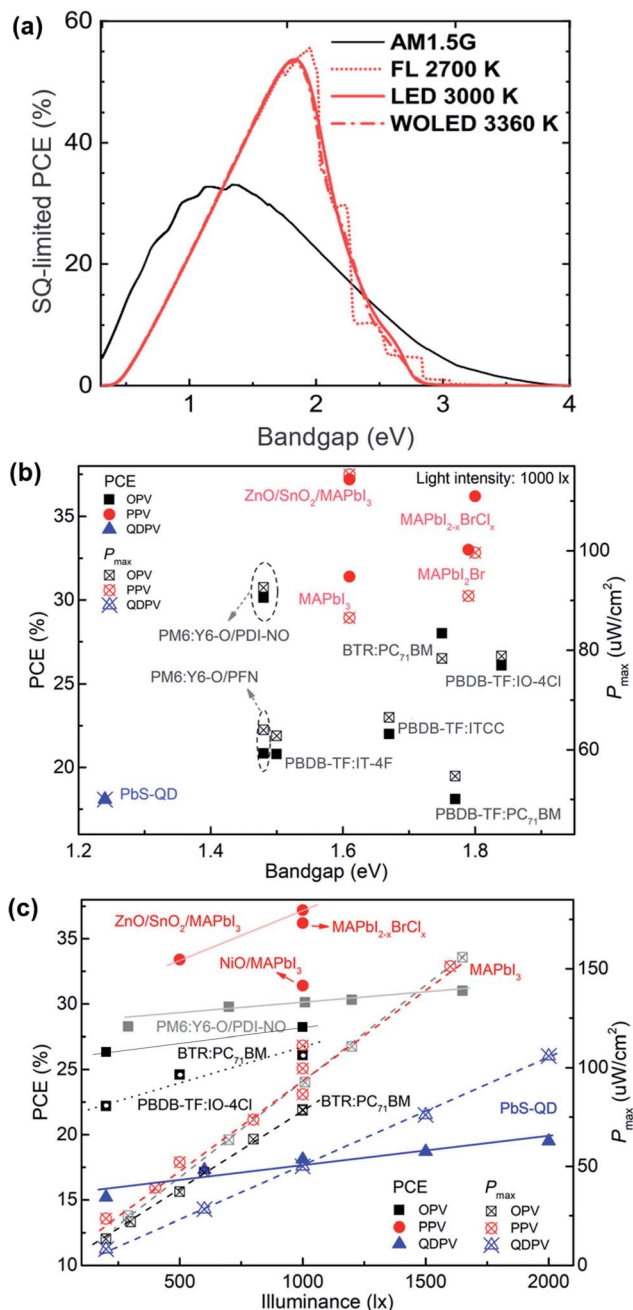


Fig. 7 (a) The Shockley–Queisser (SQ) limited PCE vs. band gap for different white light sources. The illuminance of artificial light sources is taken to be 300 lx. Adapted from ref. 87 with permission from The Royal Society of Chemistry. (b) PCE and  $P_{\max}$  of PV cells vs. acceptor bandgap under 1000 lx LED light illumination. The bandgap data was calculated from the device EQE edge of the blend film. (c) Plot of PCE and  $P_{\max}$  of different types of indoor PV cells with increasing light intensity. Data from ref. 9, 17, 28 and 31 for OPVs, ref. 10, 51 and 53 for PPVs and ref. 11 for QDPVs.

noted, however, that in addition to an optimal bandgap, device architecture and type of materials also play an important role in device performance as evidenced by the superior PCE of the PM6:Y6-O blend with the PDI-NO interlayer and MAPbI<sub>3</sub> PPVs with the SnO<sub>2</sub>/ZnO double ETL, and by the big performance difference between BTR:PC<sub>71</sub>BM and PBDB-TF:PC<sub>71</sub>BM. It is



Table 4 Device parameters of representative outstanding indoor OPV, PPV and QDPV devices under 1000 lx LED/FL light

Device	Light source at 1000 lx	$V_{oc}$ (V)	$J_{sc}$ ( $\mu\text{A cm}^{-2}$ )	FF (%)	$P_{max}$ ( $\mu\text{W cm}^{-2}$ )	PCE (%)	Ref.
BTR:PC <sub>71</sub> BM	FL	0.79	133.1	75.2	78.3	28	31
PBDB-TF:IO-4Cl	LED	1.1	90.6	79.1	78.8	26.1	17
PM6:Y6-O/PDI-NO	LED (1010 lx)	0.83	147	76	96.2	30.1	9
MAPbI <sub>2-x</sub> BrCl <sub>x</sub>	FL	1.028	126.2	76.8	99.6	36.2	51
MAPbI <sub>3-x</sub> Br <sub>x</sub>	LED	0.82	170.8	68.8	96.4	34.5	52
ZnO/SnO <sub>2</sub> /MAPbI <sub>3</sub>	LED	0.98	157.6	72	115.3	37.2	10
PbS-QD	FL	0.34	213.3	69	50	18.1	11

expected that the device performance of all three types of indoor PV technologies will continue to improve significantly with the rapid advances both in the materials and device design.

## 3 Scientific and industrial challenges

### 3.1 Standards of PV measurements

**3.1.1 Measurement of incident light.** Unlike 1 sun measurement which has a widely established standard condition (*e.g.* AM1.5G) for PV testing, there is no testing standard for indoor PV testing. Minnaert *et al.* simulated the indoor performance based on the EQE of representative devices from different PV technologies and concluded that indoor lighting can be classified into three categories:<sup>88</sup> (i) incandescent lighting and halogen lamps; (ii) broad-band fluorescent lamps and metal halide lamps; (iii) cool white FL lamps, warm and cool LEDs, and high-pressure sodium lamps. It is suggested that testing of PV devices under one type of light source in each category (*e.g.* cool LEDs which belongs to category (iii)) can represent the performances of the PV devices under other types of light sources in the same category (for category (iii), it includes warm LEDs, FL lamps and high-pressure sodium lamps). Thanks to the significant developments in the lighting industry, commonly used indoor light sources are usually very energy efficient, and emit mainly within the visible region (see Fig. 8a for the emission spectra).<sup>89</sup>

Once the light source is decided, accurate light intensity calibration is a further consideration. Other than the normal

irradiance measurements ( $\text{mW cm}^{-2}$ ) for PCE calculation, illuminance measurements, typically by using a lux meter, are also required as they describe brightness based on human eye perception which is wavelength dependent. To convert irradiance into illuminance, a wavelength-weighted factor – luminosity factor  $Y(\lambda)$  is involved in the calculation which describes human eye responses to a particular wavelength.<sup>2</sup> The equation of the conversion is shown in eqn (1) and (2).

$$L = K_r P_{in} \int_{360}^{830} S_{norm}(\lambda) Y(\lambda) d\lambda \quad (1)$$

$$S_{norm}(\lambda) = S(\lambda) / \int_0^{\infty} S(\lambda) d\lambda \quad (2)$$

where  $L$  is illuminance,  $K_r = 683.002 \text{ lm/W}$  is the maximum spectral efficacy,  $P_{in}$  is the incident power intensity,  $S(\lambda)$  is the measured spectrum of the light source,  $S_{norm}(\lambda)$  is the spectral power distribution of  $S(\lambda)$  under normalisation conditions, and  $Y(\lambda)$  is the luminosity factor. Ho *et al.* recently worked out the  $P_{in} - L$  conversion for the light sources as shown in Fig. 8b.<sup>87</sup>

Instead of performing accurate measurements of the spectrum and intensity of the indoor light source, Hamadani *et al.* proposed using a calibrated reference cell to test the light intensity levels for a given reference spectrum of the indoor light source, which is similar to the routine calibration of 1 sun measurements currently adopted in most laboratories. By this method, researchers are able to calibrate the light intensity levels simply by using the reference cell, without the need to

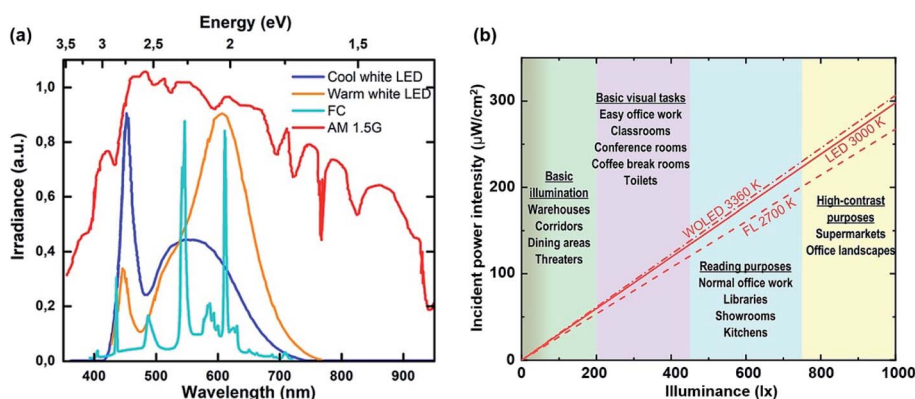


Fig. 8 (a) Spectral emission of common ambient light sources and the solar spectrum at AM 1.5G. Reproduced from ref. 89 with permission from the American Chemical Society. (b) Incident power intensity vs. illuminance for selected light sources. Reproduced from ref. 87 with permission from The Royal Society of Chemistry.



measure the absolute irradiance of the indoor light sources or the absolute quantum efficiency of the PV devices.<sup>90</sup>

**3.1.2 Measurement of photovoltaic parameters.** For indoor PV measurements,  $J_{sc}$ ,  $V_{oc}$  and FF, extracted from the  $J$ - $V$  characteristics, are usually reported. To calculate PCE,  $P_{in}$  needs to be measured. Some reports only use  $P_{max}$  to describe the performance, which is a measure of the power density generated under a given lux level without specifying how efficient the device is. As there is no standard cell for simple calibration like 1 sun, a measurement of the spectrum of the indoor light may be required to obtain the  $P_{in}$  value.

It is common to observe hysteresis in the  $J$ - $V$  scans for many types of PPV devices, where the current for a given voltage is dependent on the scan direction (forward or reverse) and scan rate. Chen *et al.* conducted an intense study on the variation of indoor performance of dye-sensitised PV devices, which is found to suffer from hysteresis, involving 15 research groups from around the world.<sup>91</sup> While there are currently very few reports on the hysteresis of PPV devices under low light conditions, the findings of Chen *et al.* suggest that the hysteresis of PPV devices could be more serious under low light conditions and a low scan rate may be required, and stabilised power generation measurements ( $P_{max}$  over time) would be a more accurate method to probe  $P_{max}$ .

Even when the indoor light sources for PV testing have been calibrated, the accuracy remains unclear, since there is no third-party calibrated reference to calibrate the light intensity similar to that for 1 sun  $J$ - $V$  measurements. Therefore, it is important to perform integration of the EQE spectrum to the indoor

spectrum as a check of the obtained  $J_{sc}$  value. However, such a check is rarely seen in the literature for indoor PVs.<sup>17,28</sup> We thereby suggest that this integration should be reported in the future.

### 3.2 Stability

Stability remains a key consideration for the commercialisation of emerging solar cells. While significant research effort has been dedicated to understanding the degradation mechanisms and enhancing the long-term stability of OPV, PPV and QDPV devices under high light (*e.g.* AM1.5G) conditions,<sup>47,92,93</sup> there are very few studies investigating their degradation behaviour under low light conditions to date, resulting in a limited understanding of their degradation mechanisms and hence a lack of materials and device design rules to achieve long term environmental stability. The very different environmental stress factors associated with low light conditions (*e.g.* lack of elevated temperatures, intensive light soaking, thermal cycling and weathering) suggest that the degradation of OPVs and PPVs under low light may be dominated by different mechanisms under high light conditions. In this section, we summarise the very recent research efforts in the stability studies of indoor OPV and PPV devices and discuss our perspectives on their degradation mechanisms under low light conditions, as well as potential strategies to address these mechanisms to enhance their long-term stability. Since QDPVs have shown excellent stability compared to OPVs and PPVs, but a comprehensive stability study of their environmental tolerance, such as moisture, heat, mechanical damage and long-time benchmark light

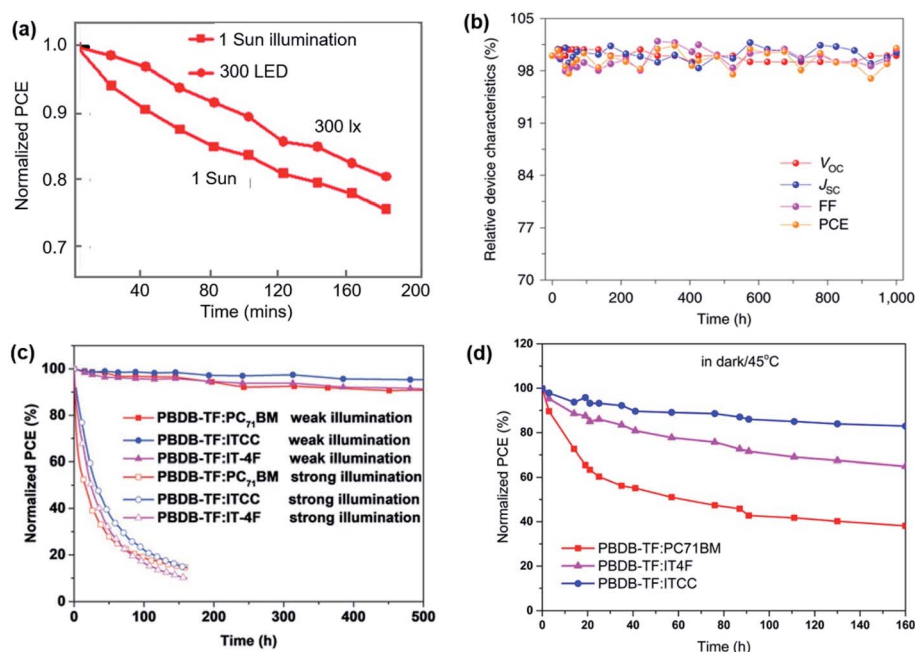


Fig. 9 (a) The stability of unencapsulated PCDTBT:PC<sub>71</sub>BM cells under 1 sun and LED. Adapted from ref. 33 with permission from The Royal Society of Chemistry. (b) Photovoltaic characteristics of an encapsulated PBDB-TF:IO-4Cl OPV device as a function of time under continuous indoor light illumination. Reproduced from ref. 17 with permission from Springer Nature. (c) The stability of three encapsulated OPV cells under continuous weak and strong illumination,<sup>28</sup> and (d) the thermal stability under 45 °C in dark.<sup>28</sup> Reproduced from ref. 28 with permission from WILEY-VCH.



soaking is seldom reported in the PV society, the stability of QDPVs under low light conditions is not included in this review.

### 3.2.1 Stability of low light OPVs

**Photochemical stability.** Photochemical degradation has been widely established as a major degradation pathway for the outdoor application of OPVs. The rapid degradation of device performance is typically triggered by a degradation of the donor and/or acceptor materials driven by the combined exposure to light and molecular oxygen, with the formation of singlet oxygen and superoxide ions, both identifying degradation mechanisms.<sup>94–96</sup> In contrast, the photochemical degradation of OPV devices under low light conditions remains significantly underexplored. Yin *et al.* compared the degradation kinetics of unencapsulated PCDTBT:PC<sub>71</sub>BM devices under outdoor (AM1.5G) and indoor (300 lx LED) conditions in air (Fig. 9a), and found that the devices under low light exhibit remarkably similar degradation kinetics to those under high light, albeit with a slightly slower rate (a 20% PCE decrease under low light and a 30% PCE decrease under high light after 180 min).<sup>33</sup> Considering the >1000 fold difference in light intensity under low light and high light conditions, the findings of Yin *et al.* suggest that the photochemical degradation of OPV devices can be triggered by very low levels of illumination, resulting in a relatively weak dependence of device photochemical stability on light intensity, which is not predictable from the accelerated lifetime testing methods currently widely established for

stability studies under high light conditions (*e.g.* predicting device lifetime by a factor of intensity multiplication), and requires significant further investigation. To avoid oxygen-induced photochemical degradation of OPV devices, a general strategy is to encapsulate the devices by using a glass or plastic layer to protect the devices from the ingress of oxygen. However, glass-based encapsulation may significantly increase the manufacturing cost, while the relatively low-cost plastic-based encapsulation is generally less effective such that it can only partially impede oxygen diffusion. The development of an effective encapsulation technology with a low fabricate cost is still a substantial challenge for merging indoor PV technologies. Apart from oxygen-induced photochemical degradation, intrinsic chemical reactions of the constituent materials (without the involvement of oxygen) are an additional degradation pathway for indoor OPVs. For example, Wang *et al.* have recently reported that the interfacial chemical reaction between the PEDOT:PSS HTL and the ITIC NFA (revealed by Raman spectroscopy) can cause the degradation of PBDB-T:ITIC-based OPVs in an ambient indoor environment (Fig. 10a and b). This degradation mechanism is found to be effectively mitigated through a passivated MoO<sub>3</sub> layer,<sup>93</sup> suggesting that the development of suitable interlayers with excellent compatibility with the rapidly advancing materials and device designs of indoor OPVs is also an important consideration to ensure their long term stability.



**Fig. 10** (a) The normalised  $V_{oc}$  measured under 1 sun as a function of aging time.<sup>93</sup> (b) Raman spectra measured for the pure PEDOT:PSS layer and the bilayer PEDOT:PSS/ITIC. Adapted from ref. 93 with permission from WILEY-VCH. (c) Evolution of  $V_{oc}$ , FF,  $J_{sc}$  and PCE of optimised PCE11:PCBM solar cells measured under continuous 1 sun in a N<sub>2</sub> atmosphere for 450 h.<sup>97</sup> (d) Evolution of  $J_{sc}$  of optimised PCE11:PCBM solar cells measured at different temperatures. Reproduced from ref. 97 under a Creative Commons Attribution 4.0 International License.



**Strong illumination and high temperature.** “Burn-in” behaviour can be observed when OPV devices operate in inert atmospheres under a continuous illumination, which represents a rapid drop of device performance within the first tens to hundreds of hours, further followed by a moderate decrease of device performance in the longer term.<sup>92</sup> Li *et al.* demonstrated a strong burn-in degradation in PCE10:PCBM-based devices (Fig. 10c) under outdoor conditions, which is attributed to the demixing of the donor and acceptor phases caused by the low miscibility between the donor and acceptor. Notably, burn-in degradation due to spontaneous phase separation in the mixed amorphous regimes is found to occur at room temperature (Fig. 10d) and even in the dark.<sup>97</sup> This study therefore shows that spinodal demixing of the active materials may be a critical issue for the stability of OPVs under low light conditions, which can be effectively mitigated by ensuring good miscibility and compatibility between the donor and acceptor. Cui *et al.* investigated the photostability of PBDB-TF:IO-4Cl devices under low light conditions, and found that the cell maintained its initial efficiency after a 1000 hour illumination period under indoor light as shown in Fig. 9b.<sup>9</sup> The authors further compared the photostability of PBDB-TF:PC<sub>71</sub>BM, PBDB-TF:ITCC and PBDB-TF:IT-4F devices under indoor light at different intensities. The results reveal a strong dependence of the device degradation behaviour upon light intensity, with the devices under weak illumination exhibiting significantly higher stability, retaining 90% of their initial efficiencies after 500 hours of illumination (Fig. 9c).<sup>28</sup> In contrast, the cells under strong illumination exhibit strong “burn-in” behaviour, losing more than 70% of their initial PCE within the first 100 hours, partially caused by a mild thermal stress (~45 °C) during illumination as revealed by dark thermal stability tests (Fig. 9d).<sup>28</sup> While the lack of intensive light soaking and elevated temperatures may facilitate the long term stability of OPV devices under low light conditions, the development of OPV materials with improved intrinsic stability against light soaking stress, as well as OPV blends with good morphological stability against thermal stress, is still an important consideration to ensure the long term stability of OPV devices under low light conditions.

**Humidity.** Since indoor OPVs may operate in an environment with high humidity, moisture-induced degradation can be a major degradation pathway for indoor OPVs, especially unencapsulated devices. It was reported that some top electrode materials such as calcium and aluminium can react with moisture in ambient air, forming bubbles and extensive voids at the top electrode/active layer interface, which spreads inward from the edge of devices over time upon exposure to relative humidity (RH) of 75%, causing degradation in device performance. The use of PEDOT:PSS as an HTL may also result in the degradation of indoor OPVs owing to its hygroscopic nature. Moisture induced degradation can be effectively mitigated by encapsulating the devices after fabrication, using moisture stable electrodes such as silver as well as replacing PEDOT:PSS or using additives in PEDOT:PSS.<sup>98</sup> While it is reasonable to expect that indoor OPVs may share similar degradation mechanisms with outdoor OPVs under moisture conditions, further

investigations are required in order to fully understand the moisture stability of indoor OPVs.

**3.2.2 Stability of low light PPVs.** The degradation of PPVs under high light conditions have been studied extensively,<sup>47,49</sup> with a range of major degradation pathways identified in the PPV device layers (perovskite material, ETL/HTL, interlayer and electrode) under various environmental stress factors (strong light, heat, oxygen and humidity). The degradation of PPVs under low light conditions is rarely studied to date, although it is expected that some degradation pathways (*e.g.* oxygen and moisture induced degradation) may exist in both outdoor and indoor PPVs, while the relatively mild light/heat stress under low light conditions, on the other hand, may facilitate better stability compared to high light conditions owing to less ionic mobility and phase transition. Nevertheless, it is expected that some additional degradation pathways may emerge under low light conditions, which may affect the stability of PPVs significantly. For example, indoor PPVs cannot generate as many photoelectrons as those under high light to fill in the pre-existing trap states owing to the lower light intensity of indoor conditions, which may accelerate device degradation. Further investigations are therefore essential to fully understand the degradation mechanisms and enhance the stability of indoor PPVs.

**Perovskite layer.** The perovskite photoactive layer plays a crucial part in the long-term stability of indoor PPVs. It has been established that the stability (under ambient/inert, dark/light, thermal/room-temperature conditions) of the perovskite layer can be significantly enhanced through composition engineering of the cation and anion elements, as well as through processing additives, antisolvent engineering and defect management.<sup>99</sup>

For example, it has recently been demonstrated that triple-halide tailored MAPbI<sub>2-x</sub>BrCl<sub>x</sub> PPV devices can sustain over 95% of their initial efficiency under continuous light soaking under 1000 lx FL light for over 2000 h,<sup>51</sup> while MAPbI<sub>3</sub> and MAPbI<sub>2</sub>Br reference devices undergo significant degradation. This is due to the key role of the small Cl<sup>-</sup> ions in causing the shrinkage in the perovskite crystal lattice and further retarding ion migration and halide segregation. To obtain a stable perovskite phase, the adoption of mixed cation perovskites or inorganic perovskites has been established as a promising strategy under 1 sun condition,<sup>49,50</sup> which may be also effective in the stability enhancement of indoor PPVs.<sup>100,101</sup> Singh *et al.* reported that the Cs-tuned Cs<sub>x</sub>(FA<sub>0.83</sub>MA<sub>0.17</sub>)<sub>(1-x)</sub>Pb(I<sub>0.83</sub>Br<sub>0.17</sub>)<sub>3</sub> (where *x* is the mole fraction of Cs) perovskite devices can achieve an optimal PCE of ~17% under AM1.5G condition when *x* = 0.05 and should also obtain decent device performance under low light conditions considering its extraordinary stability in the ambient atmosphere.<sup>101</sup> This mixed-halide PPV device showed no significant degradation in device performance upon exposure to ambient air under dark conditions with RH 20–35% (see Fig. 11a) for 18 weeks. This enhanced stability was found to originate from the absence of impurity phases after addition of Cs, in conjunction with improved perovskite crystallinity as indicated by XRD analysis (inset of Fig. 11a).





Furthermore, processing additive engineering is also found to be an effective strategy in enhancing the stability of PPVs owing to their positive impact on perovskite crystallinity and

morphology. For example, it was found that when a dimethyl sulfide (DS) additive is introducing into MAPbI<sub>3</sub>, the resulting PPVs had exhibited higher tolerance to oxygen and humidity,

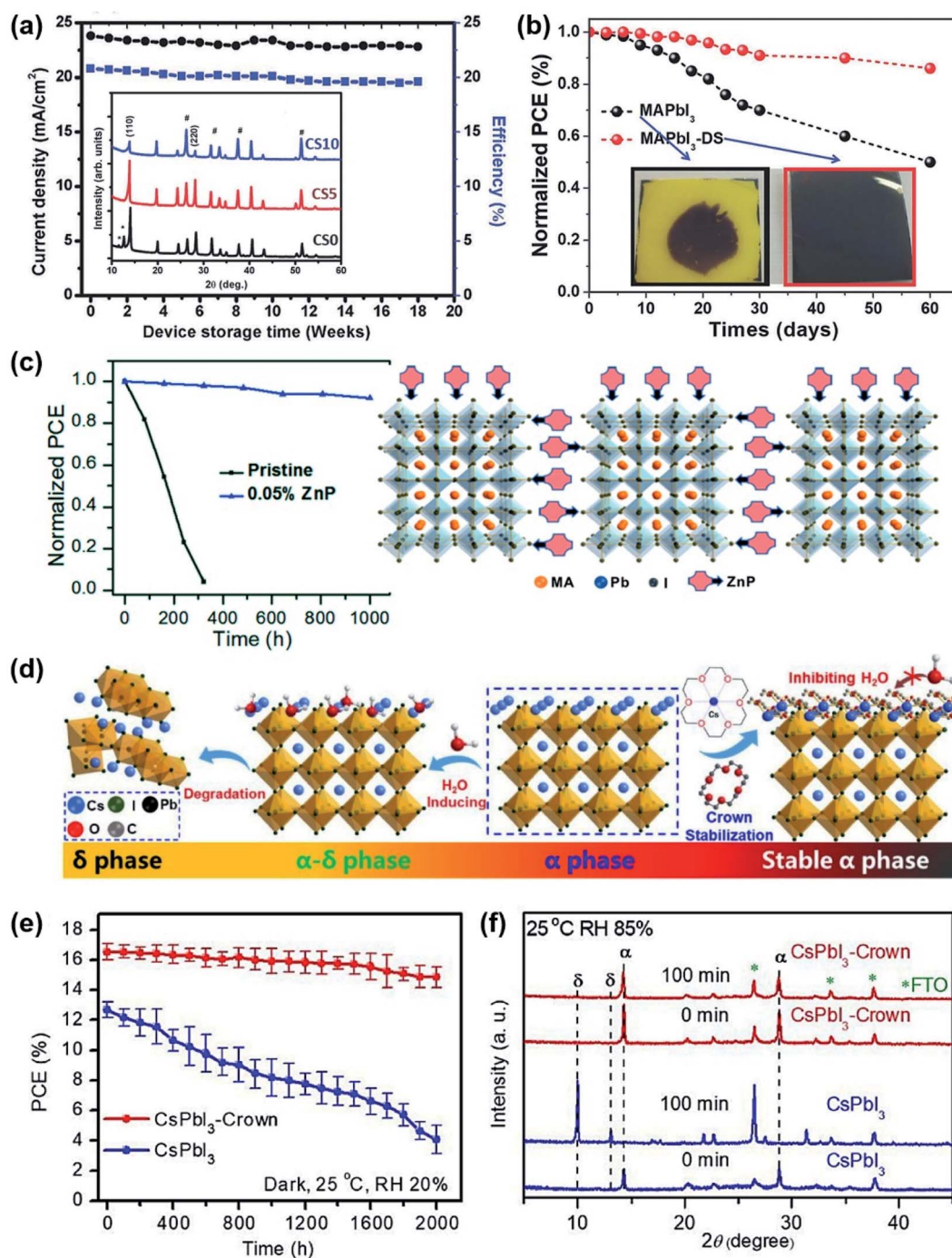


**Fig. 11** (a) Long term stability in device efficiency and current density with respect to device storage time in weeks under ambient conditions with RH 20–35%. The inset is the XRD of a Cs-tuned perovskite with Cs concentration  $x = 0$  (Cs0), 0.05 (Cs5) and 0.1 (Cs10). Adapted from ref. 101 with permission from WILEY-VCH. (b) The stability measurements of the MAPbI<sub>3</sub> and MAPbI<sub>3</sub>-DS devices exposed to ambient air at 35% humidity in the dark. Inset displays the photograph of the perovskite films after being stored for 60 days at the same condition. Reproduced from ref. 59 with permission from WILEY-VCH. (c) The stability measurements of the pristine and 0.05% ZnP-encapsulated MAPbI<sub>3</sub> devices (85 °C, RH 45%) and the structure of perovskite encapsulated by ZnP. Adapted from ref. 102 with permission from the American Chemical Society. (d) Schematic illustration of Crown passivating the surface of  $\alpha$ -CsPbI<sub>3</sub>, compared to the phase transition from  $\alpha$ -CsPbI<sub>3</sub> to  $\delta$ -CsPbI<sub>3</sub>.<sup>100</sup> (e) Storage stability of unencapsulated CsPbI<sub>3</sub>-Crown and CsPbI<sub>3</sub> devices in a chamber with constant temperature and humidity.<sup>100</sup> (f) XRD patterns of CsPbI<sub>3</sub>-Crown and CsPbI<sub>3</sub> films in the ambient atmosphere at  $\sim$ RH 85% with different aging times.<sup>100</sup> Reproduced from ref. 100 with permission from The Royal Society of Chemistry.



showing little degradation after 60 days (under dark ambient conditions, RH  $\sim$  35%, without encapsulation), while significant degradation is seen in pure MAPbI<sub>3</sub> films as indicated by loss of absorbance (film yellowing, see Fig. 11b).<sup>59</sup> This is due to the reaction of DS with Pb<sup>2+</sup> to form a chelated intermediate, which further slows down the perovskite crystallisation rate to form large grain size and good crystallinity. Li *et al.* embedded the monoammonium zinc porphyrin (ZnP) compound into the MA<sup>+</sup> lead iodide perovskite film and the resulting PPV devices showed enhanced moisture and thermal stability retaining over 90% of initial efficiency after 1000 h at 85 °C and 45% relative humidity in a N<sub>2</sub> atmosphere (Fig. 11c).<sup>102</sup> The significantly improved stability is attributed to the molecular encapsulation effect, where ZnP compounds were found to be attached on the surface of the perovskite nucleus, thereby mediating the crystallisation process and passivating the defects at the perovskite grain boundaries (Fig. 11c). Similarly, Chen *et al.* proposed a surface passivation method of drop-casting an 18-crown-6 ether (Crown) film on the CsPbI<sub>3</sub> film surface.<sup>100</sup> As shown in Fig. 11d, pristine  $\alpha$ -phase CsPbI<sub>3</sub> has high sensitivity to humidity, transferring to the  $\alpha$ - $\delta$ - or  $\delta$ -phases with H<sub>2</sub>O molecules attacking the surface. After introducing the Crown molecules, whose inner cavity can bond strongly and selectively with Cs<sup>+</sup> ions, the surface defects can be passivated. Simultaneously, the Crown-terminated CsPbI<sub>3</sub> exhibits a methylene (-CH<sub>2</sub>) outer structure on the surface, helping to enhance the moisture tolerance and thus inhibit the phase transformation. The device stability tests (Fig. 11e) show that the obtained high-quality CsPbI<sub>3</sub>-Crown devices had maintained  $\sim$ 90% of their initial PCE for up to 2000 h without encapsulation (under dark, 25 °C, RH 20%), while reference CsPbI<sub>3</sub> devices had lost  $\sim$ 65% of their initial performance, dropping to only 4.7% after 2000 h under the same degradation environment. Under a harsher degradation condition with RH increased to 85%, the CsPbI<sub>3</sub>-Crown device can still maintain a stable  $\alpha$  phase with very little  $\delta$  phase emerging in the XRD pattern over 100 min (Fig. 11f), compared to the reference CsPbI<sub>3</sub> films where most of the  $\alpha$  phase had transferred into the  $\delta$  phase. The emerging molecular and surface encapsulation methods of the perovskite layer therefore provide a promising new route for the commercialisation of efficient and stable indoor PPVs.

**ETL and HTL.** ETL and HTL also play a critical role in the stability of PPV devices. The widely used spiro-OMeTAD HTL in PPV devices usually requires additives to enhance device performance, while the common dopant lithium bis(trifluoromethanesulfonyl)imide (Li-TFSI) is hygroscopic resulting in high sensitivity to moisture. Pham *et al.* proposed to replace the Li-TFSI with the more hydrophobic alkaline-earth TFSI additives, such as Mg-TFSI<sub>2</sub> and Ca-TFSI<sub>2</sub>, which can enhance moisture-resistance of the HTL layer and help to maintain 83% efficiency of the unencapsulated devices after aging in ambient air (RH 55–70%) for 193 days.<sup>103</sup> To counter the stability related problems of HTL, a low-cost dopant-free 2,3-bis(4'-(bis(4-methoxyphenyl)amino)-[1,1'-biphenyl]-4-yl)fumaronitrile (TPA-BPFN-TPA) HTL with a water repellent property (contact angle of 112°) was recently developed.<sup>104</sup> The TPA-BPFN-TPA-based PPV devices not only exhibited significantly improved device

performance compared to spiro-OMeTAD-based PPV devices under low-light conditions (30% PCE at 1000 lx), but also improved device moisture stability under dark conditions with RH = 70% (PCE dropped from 18.4% to 8% in 100 h vs. 16.5% to 5% in 40 h). Jagadamma *et al.* developed an ultrathin HTL based on solution-processed NiO nanoparticles instead of PEDOT:PSS for indoor PPV devices, achieving a PCE of 23% under compact fluorescent lighting (0.32 mW cm<sup>-2</sup>).<sup>105</sup> After 3.7 months under ambient air conditions (in the dark, RH  $\sim$  40%), the perovskite layer on the NiO HTL still retained its initial black-brown colour while the ones on PEDOT:PSS turned yellowish implying a severe loss of absorbance. The above mentioned (in Section 2.2.1) SnO<sub>2</sub>/MgO<sup>55</sup> and PCBM/[BMIM]BF<sub>4</sub> (ref. 57) based PPV devices, which exhibited higher PCEs than their reference devices under low light, also showed improved stability due to ETL/interlayer modification which leads to efficient passivation of surface trap states and less permeation of moisture and oxygen into the perovskite layer. Upon storage in air under dark for 107 days without encapsulation, the SnO<sub>2</sub>/MgO ETL/interlayer based MAPbI<sub>3</sub> PPV devices maintained 68% of their initial efficiency, whereas those with only a SnO<sub>2</sub> ETL maintained 53% after undergoing the same degradation period. The XRD patterns of the MAPbI<sub>3</sub> films covered with PCBM/[BMIM]BF<sub>4</sub> exhibited a pure MAPbI<sub>3</sub> phase after 190 h of aging, while the PCBM/BCP-covered perovskite film displayed an additional peak in the XRD pattern corresponding to the formation of PbI<sub>2</sub>, implying a partial decomposition of MAPbI<sub>3</sub> due to the invasion of moisture and oxygen. To further increase the water resistance, Sidhik *et al.* proposed to insert a hydrophobic PbS QD layer between the perovskite layer and HTL. Compared with the significantly degraded reference MAPbI<sub>3</sub> devices after 10 days under dark ambient conditions with higher humidity of 70%, the devices utilising a PbS QD barrier layer showed less degradation (retaining 76% of their initial efficiency) after being stored for 60 days under the same environmental conditions.<sup>106</sup>

**Top electrode.** The commonly used metal electrodes (Au and Ag) for PPV devices are also important factors contributing to device degradation due to the diffusion of Au and reactivity of Ag with halide ions,<sup>47</sup> which is also expected to exist in indoor PPVs. For better compatibility with indoor IoT application, alternative low-cost and nonreactive substitutes such as hydrophobic and abundant carbon-based materials were explored as reviewed in the literature.<sup>107</sup> The carbon-based PPV devices show superior stability than the metal-electrode devices under both moisture and high-temperature environments. Although the carbon materials usually exhibit lower conductivity, the resulting PPV device with a carbon electrode still generates decent  $P_{\text{max}}$  under low light intensity.<sup>56</sup>

### 3.3 Ecotoxicity

Since low light PVs are mainly targeting indoor and portable applications (IoTs, household products, wearable electronics and biomedical devices), ecotoxicity is a vital consideration for their materials and device design, and toxic/harmful elements should be avoided or properly controlled in order to minimise



their ecotoxicity and meet the relevant safety regulations (*e.g.* RoHS) for their commercialisation. While there are relatively less concerns over the ecotoxicity of OPV devices (*e.g.* the use of heavy-metal atoms in the donor and acceptor materials<sup>17,28,108</sup> with limited risk of chemical leach), ecotoxicity is a more serious consideration for the commercialisation of PPV and QDPV devices. A recent research study revealed that the Pb from halide perovskites is more harmful than initially expected, and is 10 times more bioavailable than other sources of lead contaminants that already exist around human life.<sup>109</sup> Therefore, lead-free perovskites (*e.g.* Sn-, Ge- and all-inorganic based) and QDPVs (*e.g.* AgBiS<sub>2</sub>-based)<sup>110</sup> are more desirable than their lead-based counterparts for low light applications.<sup>46,111</sup> It should be noted, however, that lead-free PV devices typically possess lower performances and therefore still require substantial further development. To mitigate this issue, Li *et al.*<sup>112</sup> developed an on-device lead sequestration strategy based on lead-based PPVs to effectively prevent the leakage of lead in order to minimise their ecotoxicity (Fig. 12a). The authors deposited transparent P,P'-di(2-ethylhexyl) methanediphosphonic acid (DMDP) outside the FTO glass to absorb Pb and an opaque ethylenediamine tetra (methylene phosphonic acid) (EDTMP) layer as Pb-sequestering material on the device back side, which can together absorb 96% of Pb leaked upon device damage. These layers do not impact device performance and stability as indicated in Fig. 12b and c. Furthermore, the development of environment friendly materials and green fabrication procedures is also an important consideration for low light PVs. For example, PPVs typically employ DMSO and

DMF as the solvents for precursor processing,<sup>56</sup> which are not only toxic but also miscible with water, resulting in increased bioavailability in particular for large-area PPV processing in ambient environments. Reducing the use of toxic solvents and developing green solvents without compromising perovskite film quality are important considerations for their future commercialisation. Wang *et al.* developed a series of co-solvents based on the less toxic DMSO, 2-methylpyrazine (2-MP) and 1-pentanol (1-P) and achieved a stabilized PCE of up to 16%.<sup>113</sup> It has recently been demonstrated that water can be used in the fabrication of CsPbBr<sub>3</sub> PPVs.<sup>114</sup>

### 3.4 Others

Compared with outdoor light, common indoor light sources not only have different spectrum and irradiance intensities but also contain both oblique direct light and isotropic diffuse light,<sup>115</sup> which have been rarely considered in current PV studies and may impose a challenge in the standardisation of indoor testing of PV devices. Rational materials and device design of PV devices to achieve a broad angular response may be extremely beneficial to maximise device performance under low light conditions. In addition, partial shading on the device surface is more likely to occur in a complex indoor environment, which may introduce inadvertent reverse bias to individual devices and lead to device degradation similar to that under outdoor light.<sup>116</sup> Development of PV devices robust to reverse bias conditions may be a further important consideration to achieve long term stability under low light. It should also be noted that

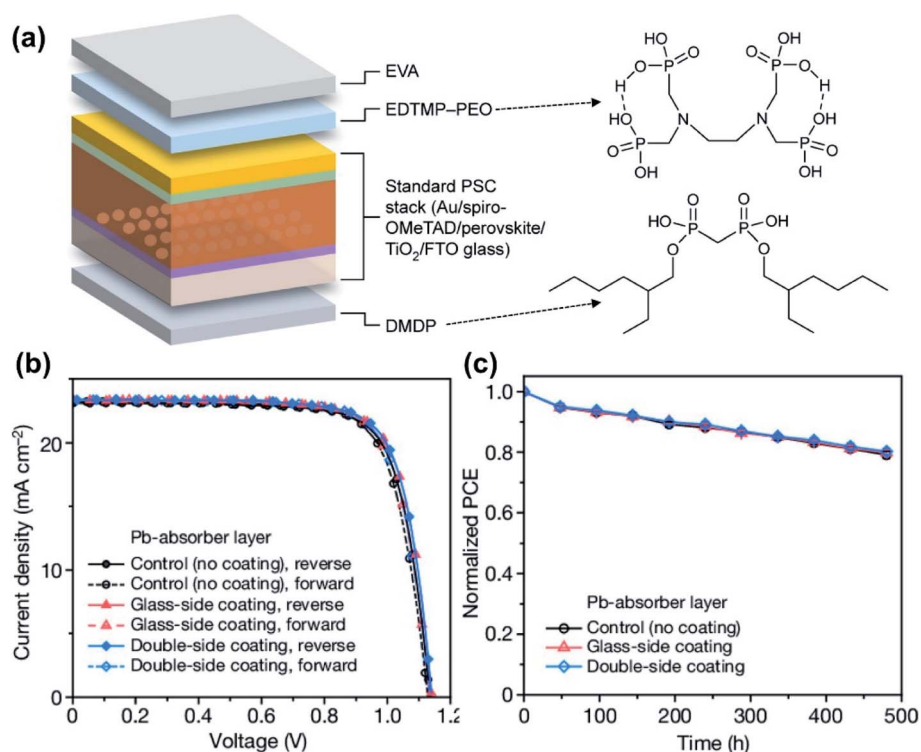


Fig. 12 (a) PPV device architecture with front and back Pb-absorbing coating layers. Comparison of the  $J$ - $V$  curves (b) and operation stability (c) for PPVs with and without the Pb-absorbing layers. Reproduced from ref. 112 with permission from Springer Nature.



indoor PVs and outdoor PVs can have very different requirements for solar cell stability and lifetimes owing to their different target applications. For example, compared to outdoor applications (e.g. power plants, building-integrated PV applications) that typically require a PV device lifetime of more than 25 years, indoor PV applications may require a much shorter PV device lifetime (e.g. integration with consumer electronics or wireless sensors, which have a typical lifespan of less than 3–5 years), suggesting that solution-processed solar cells have tremendous commercialisation potential for indoor applications and may achieve commercialisation ahead of outdoor PVs. Finally, ensuring a low production cost to adapt the market requirement (such as low price sensors) is necessary in order to maximise the commercialisation potential of solution-processed solar cells as a competitive PV technology for low light applications.

## 4 Summary

In this review, we have summarised the latest research progress on the development of solution-processed organic, perovskite and quantum dot semiconductors and devices targeting indoor PV applications. With outstanding device performance and lifetimes already achieved to date, these emerging PV technologies have demonstrated tremendous potential toward developing into a commercially viable product for use in a broad range of indoor PV applications. It is expected that further rapid enhancements are achievable both in their efficiency and stability in the near future, considering that a theoretical maximum efficiency of up to 52% has been predicted for PV devices under 1000 lx cool white LEDs with a bandgap  $\sim 1.9$  eV.<sup>48</sup>

However, several substantial challenges still remain toward the commercialisation of this emerging PV technology, in particular associated with their limited stability and ecotoxicity. Overcoming these challenges requires substantial further research efforts. However, with the rapid advances in the materials and devices of these emerging PV technologies, it is envisaged that they will realise their full potential for commercialisation in the near future.

## Author contributions

XH and YW contributed equally to this work and were in charge of writing the manuscript. HL and RD contributed to writing the Standards of PV characterisation part. NM and DY contributed to part of the perovskite and quantum dot literature summary. HL, WT, ML, FZ, BH and ZL revised the content.

## Conflicts of interest

There are no conflicts to declare.

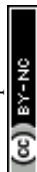
## Acknowledgements

XH, YW and ZL acknowledge the funding from the Engineering and Physical Sciences Research Council (EP/S020748/1). BH would like to acknowledge the financial support from Cardiff

University. HL, RD and WT would like to thank Airbus Endeavour Wales for the financial support and the SPECIFIC Innovation and Knowledge Centre (EP/N020863/1) for funding.

## References

- 1 H. K. H. Lee, J. Barbé and W. C. Tsoi, *Solar Cells and Light Management*, 2020, pp. 355–388.
- 2 A. Venkateswararao, J. K. Ho, S. K. So, S.-W. Liu and K.-T. Wong, *Mater. Sci. Eng., R*, 2019, **139**, 100517.
- 3 M. Otsuka, Y. Kurokawa, Y. Ding, F. B. Juangsa, S. Shibata, T. Kato and T. Nozaki, *RSC Adv.*, 2020, **10**, 12611–12618.
- 4 P. K. B. R. E. Hollingsworth and A. Madan, *J. Non-Cryst. Solids*, 1987, **97–98**, 309–312.
- 5 M. K. K. Fukutani, W. Futako, B. Kaplan, T. Kamiya, C. M. Fortmann and I. Shimizu, *J. Non-Cryst. Solids*, 1998, **227–230**, 63–67.
- 6 Y. Dai, H. Kum, M. A. Slocum, G. T. Nelson and S. M. Hubbard, *IEEE 44th Photovoltaic Specialist Conference, PVSC*, 2017, pp. 222–225.
- 7 N. Espinosa, M. Hösel, D. Angmo and F. C. Krebs, *Energy Environ. Sci.*, 2012, **5**, 5117–5132.
- 8 S. C. L. K. T. Ibn-Mohammed, I. M. Reaney, A. Acquaye, G. Schileo, K. B. Mustapha and R. Greenough, *Renewable Sustainable Energy Rev.*, 2017, **80**, 1321–1344.
- 9 L.-K. Ma, Y. Chen, P. C. Chow, G. Zhang, J. Huang, C. Ma, J. Zhang, H. Yin, A. M. H. Cheung and K. S. Wong, *Joule*, 2020, **4**, 1486–1500.
- 10 Y. W. Noh, I. S. Jin, K. S. Kim, S. H. Park and J. W. Jung, *J. Mater. Chem. A*, 2020, **8**, 17163–17173.
- 11 B. Hou, B.-S. Kim, H. K. H. Lee, Y. Cho, P. Giraud, M. Liu, J. Zhang, M. L. Davies, J. R. Durrant, W. C. Tsoi, Z. Li, S. D. Dimitrov, J. I. Sohn, S. Cha and J. M. Kim, *Adv. Funct. Mater.*, 2020, 2004563.
- 12 I. Mathews, S. N. Kantareddy, T. Buonassisi and I. M. Peters, *Joule*, 2019, **3**, 1415–1426.
- 13 J. Kalowekamo and E. Baker, *Sol. Energy*, 2009, **83**, 1224–1231.
- 14 Z. Song, C. L. McElvany, A. B. Phillips, I. Celik, P. W. Krantz, S. C. Wathage, G. K. Liyanage, D. Apul and M. J. Heben, *Energy Environ. Sci.*, 2017, **10**, 1297–1305.
- 15 D. C. Bobela, L. Gedvilas, M. Woodhouse, K. A. W. Horowitz and P. A. Basore, *Prog. Photovoltaics*, 2017, **25**, 41–48.
- 16 Y. Cui, H. Yao, J. Zhang, K. Xian, T. Zhang, L. Hong, Y. Wang, Y. Xu, K. Ma and C. An, *Adv. Mater.*, 2020, **32**, 1908205.
- 17 Y. Cui, Y. Wang, J. Bergqvist, H. Yao, Y. Xu, B. Gao, C. Yang, S. Zhang, O. Inganäs and F. Gao, *Nat. Energy*, 2019, **4**, 768–775.
- 18 R. Steim, T. Ameri, P. Schilinsky, C. Waldauf, G. Dennler, M. Scharber and C. J. Brabec, *Sol. Energy Mater. Sol. Cells*, 2011, **95**, 3256–3261.
- 19 B. P. Lechêne, M. Cowell, A. Pierre, J. W. Evans, P. K. Wright and A. C. Arias, *Nano Energy*, 2016, **26**, 631–640.
- 20 S. R. Cowan, A. Roy and A. J. Heeger, *Phys. Rev. B: Condens. Matter Mater. Phys.*, 2010, **82**, 245207.



- 21 L. J. A. Koster, V. D. Mihailetschi, R. Ramaker and P. W. Blom, *Appl. Phys. Lett.*, 2005, **86**, 123509.
- 22 Y. Wang, B. Wu, Z. Wu, Z. Lan, Y. Li, M. Zhang and F. Zhu, *J. Phys. Chem. Lett.*, 2017, **8**, 5264–5271.
- 23 H. K. Lee, Z. Li, J. R. Durrant and W. C. Tsoi, *Appl. Phys. Lett.*, 2016, **108**, 253301.
- 24 S. Mori, T. Gotanda, Y. Nakano, M. Saito, K. Todori and M. Hosoya, *Jpn. J. Appl. Phys.*, 2015, **54**, 071602.
- 25 B. Xiao, P. Calado, R. C. I. MacKenzie, T. Kirchartz, J. Yan and J. Nelson, *Phys. Rev. Appl.*, 2020, **14**, 024034.
- 26 S. S. Yang, Z. C. Hsieh, M. L. Keshtov, G. D. Sharma and F. C. Chen, *Sol. RRL*, 2017, **1**, 1700174.
- 27 Y. J. You, C. E. Song, Q. V. Hoang, Y. Kang, J. S. Goo, D. H. Ko, J. J. Lee, W. S. Shin and J. W. Shim, *Adv. Funct. Mater.*, 2019, **29**, 1901171.
- 28 Y. Cui, H. Yao, T. Zhang, L. Hong, B. Gao, K. Xian, J. Qin and J. Hou, *Adv. Mater.*, 2019, **31**, 1904512.
- 29 M. Freunek, M. Freunek and L. M. Reindl, *IEEE Journal of Photovoltaics*, 2012, **3**, 59–64.
- 30 Z. Ding, R. Zhao, Y. Yu and J. Liu, *J. Mater. Chem. A*, 2019, **7**, 26533–26539.
- 31 H. K. H. Lee, J. Wu, J. Barbé, S. M. Jain, S. Wood, E. M. Speller, Z. Li, F. A. Castro, J. R. Durrant and W. C. Tsoi, *J. Mater. Chem. A*, 2018, **6**, 5618–5626.
- 32 R. Singh, S.-C. Shin, H. Lee, J. W. Shim, K. Cho and J.-J. Lee, *Chem.–Eur. J.*, 2019, **25**, 6154–6161.
- 33 H. Yin, J. K. W. Ho, S. H. Cheung, R. J. Yan, K. L. Chiu, X. Hao and S. K. So, *J. Mater. Chem. A*, 2018, **6**, 8579–8585.
- 34 Y. Cho, T. Kumari, S. Jeong, S. M. Lee, M. Jeong, B. Lee, J. Oh, Y. Zhang, B. Huang and L. Chen, *Nano Energy*, 2020, **75**, 104896.
- 35 M. Nam, H. Y. Noh, J. Cho, Y. Park, S. C. Shin, J. A. Kim, J. Kim, H. H. Lee, J. W. Shim and D. H. Ko, *Adv. Funct. Mater.*, 2019, **29**, 1900154.
- 36 H. Yin, S. Chen, S. H. Cheung, H. W. Li, Y. Xie, S. W. Tsang, X. Zhu and S. K. So, *J. Mater. Chem. C*, 2018, **6**, 9111–9118.
- 37 S.-C. Shin, C. W. Koh, P. Vincent, J. S. Goo, J.-H. Bae, J.-J. Lee, C. Shin, H. Kim, H. Y. Woo and J. W. Shim, *Nano Energy*, 2019, **58**, 466–475.
- 38 R. Arai, S. Furukawa, Y. Hidaka, H. Komiyama and T. Yasuda, *ACS Appl. Mater. Interfaces*, 2019, **11**, 9259–9264.
- 39 R. Arai, S. Furukawa, N. Sato and T. Yasuda, *J. Mater. Chem. A*, 2019, **7**, 20187–20192.
- 40 V. V. Brus, J. Lee, B. R. Luginbuhl, S. J. Ko, G. C. Bazan and T. Q. Nguyen, *Adv. Mater.*, 2019, **31**, 1900904.
- 41 H. Yin, J. K. W. Ho, V. Piradi, S. Chen, X. Zhu and S. K. So, *Small Methods*, 2020, **4**, 2000136.
- 42 B. R. Lee, J. S. Goo, Y. W. Kim, Y.-J. You, H. Kim, S.-K. Lee, J. W. Shim and T. G. Kim, *J. Power Sources*, 2019, **417**, 61–69.
- 43 NationalRenewableEnergyLaboratory, *Best Research-Cell Efficiency*, 2020.
- 44 K. X. Steirer, P. Schulz, G. Teeter, V. Stevanovic, M. Yang, K. Zhu and J. J. Berry, *ACS Energy Lett.*, 2016, **1**, 360–366.
- 45 C. Y. Chen, J. H. Chang, K. M. Chiang, H. L. Lin, S. Y. Hsiao and H. W. Lin, *Adv. Funct. Mater.*, 2015, **25**, 7064–7070.
- 46 P.-K. Kung, M.-H. Li, P.-Y. Lin, J.-Y. Jhang, M. Pantaler, D. C. Lupascu, G. Grancini and P. Chen, *Sol. RRL*, 2020, **4**, 1900306.
- 47 S. P. Dunfield, L. Bliss, F. Zhang, J. M. Luther, K. Zhu, M. F. van Hest, M. O. Reese and J. J. Berry, *Adv. Energy Mater.*, 2020, **10**, 1904054.
- 48 G. Jarosz, R. Marczyński and R. Signerski, *Mater. Sci. Semicond. Process.*, 2020, **107**, 104812.
- 49 Q. Fu, X. Tang, B. Huang, T. Hu, L. Tan, L. Chen and Y. Chen, *Adv. Sci. c*, 2018, **5**, 1700387.
- 50 Q. Wang, N. Phung, D. Di Girolamo, P. Vivo and A. Abate, *Energy Environ. Sci.*, 2019, **12**, 865–886.
- 51 R. Cheng, C. C. Chung, H. Zhang, F. Liu, W. T. Wang, Z. Zhou, S. Wang, A. B. Djurišić and S. P. Feng, *Adv. Energy Mater.*, 2019, **9**, 1901980.
- 52 J. W. Lim, H. Kwon, S. H. Kim, Y.-J. You, J. S. Goo, D.-H. Ko, H. J. Lee, D. Kim, I. Chung, T. G. Kim, D. H. Kim and J. W. Shim, *Nano Energy*, 2020, **75**, 104984.
- 53 M. H. Ann, J. Kim, M. Kim, G. Alosaimi, D. Kim, N. Y. Ha, J. Seidel, N. Park, J. S. Yun and J. H. Kim, *Nano Energy*, 2020, **68**, 104321.
- 54 S. Yang, H. Zhao, Y. Han, C. Duan, Z. Liu and S. Liu, *Small*, 2019, **15**, 1904387.
- 55 J. Dagar, S. Castro-Hermosa, G. Lucarelli, F. Cacialli and T. M. Brown, *Nano Energy*, 2018, **49**, 290–299.
- 56 H. K. H. Lee, J. Barbé, S. M. Meroni, T. Du, C. T. Lin, A. Pockett, J. Troughton, S. M. Jain, F. De Rossi and J. Baker, *Sol. RRL*, 2019, **3**, 1800207.
- 57 M. Li, C. Zhao, Z. K. Wang, C. C. Zhang, H. K. Lee, A. Pockett, J. Barbé, W. C. Tsoi, Y. G. Yang and M. J. Carnie, *Adv. Energy Mater.*, 2018, **8**, 1801509.
- 58 F. Di Giacomo, V. Zardetto, G. Lucarelli, L. Cinà, A. Di Carlo, M. Creatore and T. Brown, *Nano Energy*, 2016, **30**, 460–469.
- 59 J. Feng, X. Zhu, Z. Yang, X. Zhang, J. Niu, Z. Wang, S. Zuo, S. Priya, S. Liu and D. Yang, *Adv. Mater.*, 2018, **30**, 1801418.
- 60 B. Cao, L. Yang, S. Jiang, H. Lin, N. Wang and X. Li, *J. Mater. Chem. A*, 2019, **7**, 4960–4970.
- 61 F. Di Giacomo, A. Fakharuddin, R. Jose and T. M. Brown, *Energy Environ. Sci.*, 2016, **9**, 3007–3035.
- 62 H. Xie, X. Yin, Y. Guo, J. Liu, W. Que and G. Wang, *Phys. Status Solidi RRL*, 2019, **13**, 1800566.
- 63 G. Lucarelli, F. Di Giacomo, V. Zardetto, M. Creatore and T. M. Brown, *Nano Res.*, 2017, **10**, 2130–2145.
- 64 J. Dagar, S. Castro-Hermosa, M. Gasbarri, A. L. Palma, L. Cina, F. Matteocci, E. Calabrò, A. Di Carlo and T. M. Brown, *Nano Res.*, 2018, **11**, 2669–2681.
- 65 A. H. Ali, Z. Hassan and A. Shuhaimi, *Appl. Surf. Sci.*, 2018, **443**, 544–547.
- 66 S. Castro-Hermosa, G. Lucarelli, M. Top, M. Fahland, J. Fahlteich and T. M. Brown, *Cell Reports Physical Science*, 2020, **1**, 100045.
- 67 S. Kim, H. Oh, G. Kang, I. K. Han, I. Jeong and M. Park, *ACS Appl. Energy Mater.*, 2020, **3**, 6995–7003.
- 68 Z. Li, T. R. Klein, D. H. Kim, M. Yang, J. J. Berry, M. F. van Hest and K. Zhu, *Nat. Rev. Mater.*, 2018, **3**, 1–20.
- 69 N.-G. Park and K. Zhu, *Nat. Rev. Mater.*, 2020, **5**, 333–350.



- 70 J. E. Bishop, C. D. Read, J. A. Smith, T. J. Routledge and D. G. Lidzey, *Scientific reports*, 2020, **10**, 1–8.
- 71 T. Bu, X. Liu, J. Li, W. Huang, Z. Wu, F. Huang, Y.-B. Cheng and J. Zhong, *Sol. RRL*, 2020, **4**, 1900263.
- 72 F. De Rossi, J. A. Baker, D. Beynon, K. E. A. Hooper, S. M. P. Meroni, D. Williams, Z. Wei, A. Yasin, C. Charbonneau, E. H. Jewell and T. M. Watson, *Adv. Mater. Technol.*, 2018, **3**, 1800156.
- 73 B. Hou, *Isr. J. Chem.*, 2019, **59**, 637–638.
- 74 B. Li, M. Lu, J. Feng, J. Zhang, P. M. Smowton, J. I. Sohn, I.-K. Park, H. Zhong and B. Hou, *J. Mater. Chem. C*, 2020, **8**, 10676–10695.
- 75 C.-H. M. Chuang, P. R. Brown, V. Bulović and M. G. Bawendi, *Nat. Mater.*, 2014, **13**, 796–801.
- 76 Z. Ning, O. Voznyy, J. Pan, S. Hoogland, V. Adinolfi, J. Xu, M. Li, A. R. Kirmani, J.-P. Sun and J. Minor, *Nat. Mater.*, 2014, **13**, 822–828.
- 77 M. C. Beard, J. M. Luther, O. E. Semonin and A. J. Nozik, *Acc. Chem. Res.*, 2013, **46**, 1252–1260.
- 78 M. C. Beard, A. G. Midgett, M. C. Hanna, J. M. Luther, B. K. Hughes and A. J. Nozik, *Nano Lett.*, 2010, **10**, 3019–3027.
- 79 A. J. Nozik, *Annu. Rev. Phys. Chem.*, 2001, **52**, 193–231.
- 80 A. Shabaev, A. L. Efros and A. Nozik, *Nano Lett.*, 2006, **6**, 2856–2863.
- 81 Y. Bi, S. Pradhan, S. Gupta, M. Z. Akgul, A. Stavrinadis and G. Konstantatos, *Adv. Mater.*, 2018, **30**, 1704928.
- 82 B. Sun, A. Johnston, C. Xu, M. Wei, Z. Huang, Z. Jiang, H. Zhou, Y. Gao, Y. Dong, O. Ouellette, X. Zheng, J. Liu, M.-J. Choi, Y. Gao, S.-W. Baek, F. Laquai, O. M. Bakr, D. Ban, O. Voznyy, F. P. Garcia de Arquer and E. H. Sargent, *Joule*, 2020, **4**, 1542–1556.
- 83 M.-J. Choi, F. P. G. de Arquer, A. H. Proppe, A. Seifitokaldani, J. Choi, J. Kim, S.-W. Baek, M. Liu, B. Sun and M. Biondi, *Nat. Commun.*, 2020, **11**, 1–9.
- 84 B. Hou, Y. Cho, B. S. Kim, J. Hong, J. B. Park, S. J. Ahn, J. I. Sohn, S. Cha and J. M. Kim, *ACS Energy Lett.*, 2016, **1**, 834–839.
- 85 B. Hou, Y. Cho, B.-S. Kim, D. Ahn, S. Lee, J. B. Park, Y.-W. Lee, J. Hong, H. Im and S. M. Morris, *J. Mater. Chem. C*, 2017, **5**, 3692–3698.
- 86 A. Kiani, H. Fayaz Movahed, S. Hoogland, O. Voznyy, R. Wolowiec, L. Levina, F. P. Garcia de Arquer, P. Pietsch, X. Wang, P. Maraghechi and E. H. Sargent, *ACS Energy Lett.*, 2016, **1**, 740–746.
- 87 J. K. W. Ho, H. Yin and S. K. So, *J. Mater. Chem. A*, 2020, **8**, 1717–1723.
- 88 B. Minnaert and P. Veelaert, *Energies*, 2014, **7**, 1500–1516.
- 89 M. Mainville and M. Leclerc, *ACS Energy Lett.*, 2020, **5**, 1186–1197.
- 90 B. H. Hamadani and M. B. Campanelli, *IEEE Journal of Photovoltaics*, 2020, **10**, 1119–1125.
- 91 C.-Y. Chen, Z.-H. Jian, S.-H. Huang, K.-M. Lee, M.-H. Kao, C.-H. Shen, J.-M. Shieh, C.-L. Wang, C.-W. Chang and B.-Z. Lin, *J. Phys. Chem. Lett.*, 2017, **8**, 1824–1830.
- 92 Z. Li, E. Speller, J. Durrant, J.-S. Kim, W. Tsoi, A. J. Clarke, J. Luke, T. Wang, H. C. Wong and H. Lee, *J. Mater. Chem. A*, 2019, **7**, 23361–23377.
- 93 Y. Wang, W. Lan, N. Li, Z. Lan, Z. Li, J. Jia and F. Zhu, *Adv. Energy Mater.*, 2019, **9**, 1900157.
- 94 E. M. Speller, A. J. Clarke, N. Aristidou, M. F. Wyatt, L. Francàs, G. Fish, H. Cha, H. K. H. Lee, J. Luke and A. Wadsworth, *ACS Energy Lett.*, 2019, **4**, 846–852.
- 95 Z. Li, J. Nelson, H. Lee, J. Durrant, J. A. Röhr, A. Telford, M. F. Wyatt, B. Rice, J. Wu and J. McGettrick, *Energy Environ. Sci.*, 2018, **11**, 417–428.
- 96 E. M. Speller, J. D. McGettrick, B. Rice, A. M. Telford, H. K. Lee, C.-H. Tan, C. S. De Castro, M. L. Davies, T. M. Watson and J. Nelson, *ACS Appl. Mater. Interfaces*, 2017, **9**, 22739–22747.
- 97 N. Li, J. D. Perea, T. Kassar, M. Richter, T. Heumueller, G. J. Matt, Y. Hou, N. S. Güldal, H. Chen and S. Chen, *Nat. Commun.*, 2017, **8**, 14541.
- 98 T. S. Glen, N. W. Scarratt, H. Yi, A. Iraqi, T. Wang, J. Kingsley, A. R. Buckley, D. G. Lidzey and A. M. Donald, *J. Polym. Sci., Part B: Polym. Phys.*, 2016, **54**, 216–224.
- 99 H. Jin, E. Debroye, M. Keshavarz, I. G. Scheblykin, M. B. Roeflaers, J. Hofkens and J. A. Steele, *Mater. Horiz.*, 2020, **7**, 397–410.
- 100 R. Chen, Y. Hui, B. Wu, Y. Wang, X. Huang, Z. Xu, P. Ruan, W. Zhang, F. Cheng and W. Zhang, *J. Mater. Chem. A*, 2020, **8**, 9597–9606.
- 101 T. Singh and T. Miyasaka, *Adv. Energy Mater.*, 2018, **8**, 1700677.
- 102 C. Li, J. Yin, R. Chen, X. Lv, X. Feng, Y. Wu and J. Cao, *J. Am. Chem. Soc.*, 2019, **141**, 6345–6351.
- 103 N. D. Pham, J. Shang, Y. Yang, M. T. Hoang, V. T. Tiong, X. Wang, L. Fan, P. Chen, L. Kou and L. Wang, *Nano Energy*, 2020, **69**, 104412.
- 104 H. D. Pham, S. M. Jain, M. Li, Z. K. Wang, S. Manzhos, K. Feron, S. Pitchaimuthu, Z. Liu, N. Motta and J. R. Durrant, *Adv. Electron. Mater.*, 2020, **6**, 1900884.
- 105 L. K. Jagadamma, O. Blaszczyk, M. T. Sajjad, A. Ruseckas and I. D. Samuel, *Sol. Energy Mater. Sol. Cells*, 2019, **201**, 110071.
- 106 S. Sidhik, C. R. Pérez, M. A. S. Estrada, T. López-Luke, A. Torres and E. De la Rosa, *Sol. Energy*, 2020, **202**, 438–445.
- 107 M. Hadadian, J.-H. Smätt and J.-P. Correa-Baena, *Energy Environ. Sci.*, 2020, **13**, 1377–1407.
- 108 H.-I. Je, E.-Y. Shin, K. J. Lee, H. Ahn, S. Park, S. H. Im, Y.-H. Kim, H. J. Son and S.-K. Kwon, *ACS Appl. Mater. Interfaces*, 2020, **12**, 23181–23189.
- 109 J. Li, H.-L. Cao, W.-B. Jiao, Q. Wang, M. Wei, I. Cantone, J. Lü and A. Abate, *Nat. Commun.*, 2020, **11**, 1–5.
- 110 M. Bernechea, N. C. Miller, G. Xercavins, D. So, A. Stavrinadis and G. Konstantatos, *Nat. Photonics*, 2016, **10**, 521–525.
- 111 T. Miyasaka, A. Kulkarni, G. M. Kim, S. Öz and A. K. Jena, *Adv. Energy Mater.*, 2020, **10**, 1902500.
- 112 X. Li, F. Zhang, H. He, J. J. Berry, K. Zhu and T. Xu, *Nature*, 2020, **578**, 555–558.



## Review

- 113 J. Wang, F. Di Giacomo, J. Brüls, H. Gortler, I. Katsouras, P. Groen, R. A. Janssen, R. Andriessen and Y. Galagan, *Sol. RRL*, 2017, **1**, 1700091.
- 114 X. Cao, G. Zhang, L. Jiang, Y. Cai, Y. Gao, W. Yang, X. He, Q. Zeng, G. Xing and Y. Jia, *ACS Appl. Mater. Interfaces*, 2019, **12**, 5825–5931.
- 115 C. A. Reynaud, R. Clerc, P. B. Lechêne, M. Hébert, A. Cazier and A. C. Arias, *Sol. Energy Mater. Sol. Cells*, 2019, **200**, 110010.
- 116 R. A. Razera, D. A. Jacobs, F. Fu, P. Fiala, M. Dussouillez, F. Sahli, T. C. Yang, L. Ding, A. Walter and A. F. Feil, *J. Mater. Chem. A*, 2020, **8**, 242–250.

